Analytical framework for disturbance energy balance in thermoacoustic devices

Journal:	*Journal of Fluid Mechanics*
Manuscript ID	JFM-19-S-0659.R3
mss type:	JFM Papers
Date Submitted by the Author:	n/a
Complete List of Authors:	Lu, Xiaofeng; Imperial College London Martinez-Botas, Ricardo; Imperial College London Hey, Jonathan; Singapore Institute of Manufacturing Technology
Keyword:	Aeroacoustics < Acoustics, Gas dynamics < Compressible Flows

Analytical framework for disturbance energy balance in thermoacoustic devices

Xiaofeng Lu[1], Ricardo Martinez-Botas[1]†, and Jonathan Hey[2]

[1]Department of Mechanical Engineering, Imperial College London, London SW7 2AZ, UK
[2]Mechatronics group, Singapore Institute of Manufacturing Technology, Singapore 138634

(Received xx; revised xx; accepted xx)

Thermoacoustic devices represent a significant future opportunity in the fields of energy generation and refrigeration. A key component of this type of device is the regenerator, where the conversion between acoustic energy and thermal energy takes place. This conversion occurs due to an externally imposed temperature gradient on the wall of the regenerator channels. Hence, this paper concerns the physics of sound waves in the proximity of such walls. It establishes a new analytical framework which clarifies the disturbance energy conservation in thermoacoustic devices. In this framework, a thermoacoustic production term is proposed to quantify the generation or consumption of disturbance energy originated from the temperature gradient. An extended disturbance energy flux term is identified to account for wave growth or decay through the regenerator. The disturbance energy balance relation states that the disturbance energy flux equals the thermoacoustic production less the viscous and thermal dissipation resulting from gradients of fluctuating velocity and temperature. The analytical framework is implemented into an axisymmetric cylindrical domain; the two dimensional nature of this work helps to uncover that the wave always decays in the region close to the wall. A dimensional analysis is conducted to identify the controlling parameters, namely the Womersley, Helmholtz and Prandtl number. A parametric study of the Womersley and Helmholtz number is conducted to showcase the new analytical methodology; the results make it possible to optimize the geometry, wave properties and working conditions of a thermoacoustic device according to the preference of its efficiency, loss and output.

Key words:

1. Introduction

The need to reduce CO_2 emissions is transforming the energy-related sectors; new methods of production and waste heat recovery are under development to achieve the required reduction targets. Similarly much research in recent years has focused on recovering waste heat and harness renewable energy sources. Among the possible technologies, the thermoacoustic device is unique in terms of its flexibility, reliability and affordability. Any external heat (solar energy, combustion, exhaust gas, hot liquid) can be supplied to the system via heat exchangers. The need of any moving parts, such as pistons, shafts and turbo-machines, is eliminated thereby minimising friction, lubrication and wear. Thermoacoustic devices also have a simple structure which leads to reduced parts, ease of assembly and consequently low construction costs. In addition, thermoacoustic

† Email address for correspondence: r.botas@imperial.ac.uk

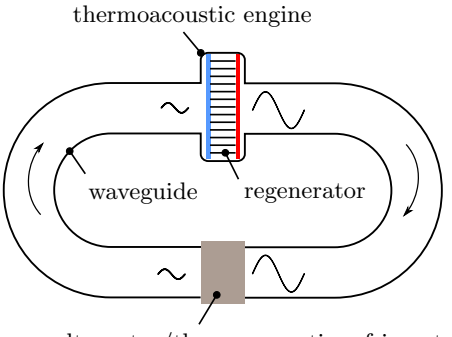

FIGURE 1. A schematic diagram of a typical travelling-wave thermoacoustic energy system. The blue and red strip denote cold and hot heat exchangers, respectively. Arrows denote the direction in which the waves propagate.

devices typically use noble gases as working fluid; these gases are environmentally-friendly and cause no greenhouse effects.

Thermoacoustic devices in this paper refer to any cyclic devices which make use of the interaction between acoustic waves and solid boundaries with a temperature gradient. In place of mechanical components, the acoustic waves provide the necessary compression and expansion process and drive the fluid to oscillate. As the fluid moves back and forth over the imposed spatial temperature difference, it absorbs and rejects heat from and to the solid wall. Depending on the sequence of heat transfer and pressure/volume change, a thermoacoustic device can accomplish either power generation or refrigeration. When the acoustic waves are externally supplied, for example by a loudspeaker, the device operates as a thermoacoustic refrigerator (e.g. Poese & Garrett 2000; Bassem *et al.* 2011) where acoustic work is consumed to transport heat against a temperature increase. If the temperature gradient is externally imposed, the device operates as a thermoacoustic engine (Backhaus & Swift 1999; Tijani & Spoelstra 2011) where the acoustic waves are spontaneously excited by the net heat input. The acoustic waves can be used for electricity generation if the engine is coupled with a linear alternator (Yu *et al.* 2012) or driving a thermoacoustic refrigerator, completing a heat-acoustic-cool conversion (Dai *et al.* 2006). A schematic diagram of a typical travelling-wave thermoacoustic energy system is shown in figure 1. The amplified waveform after going through the thermoacoustic engine indicates the conversion from thermal to acoustic energy. The diminished waveform indicates the consumption of acoustic energy by output devices such as linear alternator and thermoacoustic refrigerator. Figure 1 also that the regenerator consists of numerous narrow flow channels. This paper concerns the disturbance energy conservation in one single regenerator channel.

Thermoacoustics as a physical process exists in different systems with different characteristics, but the conversion between thermal and acoustic energy is always central to the phenomenon. In combustion systems like gas turbine engines, the thermoacoustic combustion instability is a major issues (Lieuwen & Yang 2005). The thermal energy from unsteady heat release amplifies acoustic waves (Dowling & Stow 2003), which causes damage. On the contrary, in thermoacoustic devices, the conversion is purposefully encouraged as much as possible. The conversion happens in the component called the regenerator or stack which consists of many small channels; the energy conversion is therefore subtle and complex due to the interaction of oscillations, viscosity and heat transfer. It is worth noting that often the modelling of thermoacoustic processes is

approximated using a heat transfer term and a drag term (Karpov & Prosperetti 2002; Scalo *et al.* 2015); although these terms help to model the system dynamics, the empirical method provides limited new insights into the energy conversion. The direct solution of energy conversion, in perturbation theory, requires the evaluation of at least second-order terms. Merkli & Thomann (1975) first found that in order to get the second-order time-averaged wall heat flux, only the linear solutions of temperature and axial velocity oscillation were needed. They gave the analytical expression of heat flux to the wall for a constant temperature in the resonance tube. The results showed that the local wall heat flux equals the axial change of cross-sectional enthalpy flux due to the oscillation. This idea has been further developed by Rott (1975), who included a temperature gradient on the wall.

Another approach to analyse the energy balance in thermoacoustic devices is to use the sum of all energy flux density, which is a conserved quantity for periodic oscillation (Cao *et al.* 1996). The energy balance was explained as the conversion between acoustic intensity and the product of mean density, mean temperature and local entropy flux (Swift 1988; Tominaga 1995) which was loosely termed 'thermoacoustic heat flux'. Although this theory could explain the growth of acoustic intensity, it assumes that the wall is adiabatic for second-order heat flux. Also dissipation was not included in the conversion and the role of wall temperature was not clear.

A third angle of energy analysis has been briefly mentioned by Swift (2002, pp. 109-111). Based on a lumped-element approach, it discussed the axial change of acoustic intensity in two simplified cases: zero viscosity and constant wall temperature. Although the definition of dissipation and source term are preliminary, this approach is particularly inspirational to the current study.

In other research area, there has also been some very relevant discussion. As a pure mechanics problem, the disturbance energy conservation itself has received considerable interests. Chu (1965) recognised the role of entropy fluctuation in the definition disturbance energy compared with acoustic energy. Myers (1991) has shown the disturbance energy corollary is a 'complete, consistent representation of total fluid energy conservation' at the leading order (second order) and it only contains first-order fluctuation quality. Built upon this work, Giauque *et al.* (2006) extended the disturbance energy corollary to reacting flow by including a mixture of gaseous species and heat release terms.

In summary, there is a lack of rigorous theory in the literature to explain the disturbance energy budget in conditions typically found in thermoacoustic devices:

- extreme long and narrow tubes,
- significant viscous effects,
- mean temperature gradient imposed on the solid boundary,
- significant heat transfer with the wall.

More importantly, by using the disturbance energy balance, a new perspective is enabled to look at how various parameters affect the performance and characteristics of thermoacoustic devices. This is urgently needed to make thermoacoustic devices more efficient and applicable.

This paper presents a new analytical framework by applying the disturbance energy corollary to thermoacoustic devices. A thermoacoustic production term which is directly linked to the wall temperature gradient is newly defined. In place of acoustic intensity, an extended flux term is used to account for spatial growth or decay of the energy transported by the waves. Together with viscous and thermal dissipation resulting from gradients of fluctuating velocity and temperature, the disturbance energy balance relation is then established. The analytical framework is implemented in an axisymmetric cylin-

drical domain. A dimensional analysis is conducted to reveal the controlling parameters, namely the Womersley, Helmholtz and Prandtl number. The disturbance energy terms are then simplified by using order of magnitude analysis and taking advantage of boundary conditions. The solutions and numerical scheme are then given and a global error is defined. A parametric study of the Womersley number and Helmholtz demonstrates the usage of the analytical framework and provides insights into the flow physics.

2. Analytical framework

In this section, a new analytical framework for disturbance energy balance is developed, starting with linearising and re-arranging the basic governing equations. The thermoacoustic production is rigorously defined together with an extended flux term to account for the spatial disturbance energy change. With the inclusion of dissipation mechanisms, the disturbance energy balance relation is established and the physical interpretation of the terms is given in detail.

The formulation begins with the governing equations,

$$p = \rho R_g T, \tag{2.1}$$

$$\frac{\partial \rho}{\partial t} + \nabla \cdot (\rho \boldsymbol{v}) = 0, \tag{2.2}$$

$$\rho \left[\frac{\partial \boldsymbol{v}}{\partial t} + (\boldsymbol{v} \cdot \nabla) \boldsymbol{v} \right] = -\nabla p + \nabla \cdot \boldsymbol{\tau}, \tag{2.3}$$

$$\rho T \left(\frac{\partial s}{\partial t} + \boldsymbol{v} \cdot \nabla s \right) = \nabla \cdot k \nabla T + (\boldsymbol{\tau} \cdot \nabla) \cdot \boldsymbol{v}. \tag{2.4}$$

The fluid is taken as an ideal gas and the flow as laminar. In oscillatory pipe flow, three main types of flow regimes have been observed: laminar flow, disturbed laminar flow and intermittently turbulent flow (Hino *et al.* 1976; Akhavan *et al.* 1991). The intermittently turbulence is characterized by the sudden burst into turbulence during the decelerating phase of the cycle and the subsequent reversion to laminar flow during the accelerating phase. The transition usually depends on both the Stokes parameter (the ratio of pipe radius to Stokes-layer thickness) and the Reynolds number. The maximum Stokes parameter and diameter-based Reynolds number is calculated to be 1.2 and 190, respectively, for all cases in this study. According to the criteria given by Ohmi *et al.* (1982), the flow in this study is laminar and well away from transition.

When a disturbance is present, flow variables can be decomposed into mean values, denoted by subscript 0, and fluctuation component, denoted by prime, such as $p = p_0 + p'$ and $\rho = \rho_0 + \rho'$. Assuming that the mean state is quiescent and the mean pressure is homogeneous, it follows that $\boldsymbol{v} = \boldsymbol{v}'$, $\boldsymbol{\tau} = \boldsymbol{\tau}'$, $\nabla p_0 = 0$ and $\partial f_0 / \partial t = 0$ where f is any flow variable. When the disturbance is of a small amplitude, linear approximation applies and only the first-order terms are kept. The linearised governing equations take the form,

$$p_0 = \rho_0 R_g T_0, \tag{2.5a}$$

$$p'/p_0 = \rho'/\rho_0 + T'/T_0, \tag{2.5b}$$

$$\frac{\partial \rho'}{\partial t} + \rho_0 \nabla \cdot \boldsymbol{v}' + \boldsymbol{v}' \cdot \nabla \rho_0 = 0, \tag{2.6}$$

$$\rho_0 \frac{\partial \boldsymbol{v}'}{\partial t} = -\nabla p' + \nabla \cdot \boldsymbol{\tau}', \tag{2.7}$$

$$\rho_0 T_0 \left(\frac{\partial s'}{\partial t} + \boldsymbol{v}' \cdot \nabla s_0 \right) = k \nabla^2 T', \tag{2.8}$$

where the gradient of thermal conductivity (∇k) is ignored. Multiplying (2.6) with p'/ρ_0, (2.8) with T'/T_0, taking the dot product of (2.7) with $\boldsymbol{v}'$ and adding them together yields

$$\begin{aligned} \frac{\partial}{\partial t}\left(\frac{1}{2}\rho_0 v'^2\right) + \frac{p'}{\rho_0}\frac{\partial \rho'}{\partial t} + \rho_0 T' \frac{\partial s'}{\partial t} =& -\nabla \cdot (p' \boldsymbol{v}') - \frac{p' \boldsymbol{v}'}{\rho_0} \cdot \nabla \rho_0 + \boldsymbol{v}' \cdot (\nabla \cdot \boldsymbol{\tau}) \\ &+ \frac{T'}{T_0} k \nabla^2 T' - \rho_0 T' \boldsymbol{v}' \cdot \nabla s_0. \end{aligned} \tag{2.9}$$

Using Taylor's theorem to expand thermodynamic relations $\rho = \rho(p, s)$ and $T = T(p, s)$ around mean values and again keeping only the first-order term, yields

$$\rho' = \left(\frac{\partial \rho}{\partial p}\right)_0 p' + \left(\frac{\partial \rho}{\partial s}\right)_0 s', \tag{2.10}$$

$$T' = \left(\frac{\partial T}{\partial p}\right)_0 p' + \left(\frac{\partial T}{\partial s}\right)_0 s', \tag{2.11}$$

whose coefficients can be evaluated using the definition of isentropic sound speed c, specific heat at constant pressure c_p, coefficient of thermal expansion β and thermodynamic partial differential relations. The coefficients are then written as,

$$\left(\frac{\partial \rho}{\partial p}\right)_0 = \frac{1}{c_0^2}, \qquad \left(\frac{\partial \rho}{\partial s}\right)_0 = -\frac{\rho_0 \beta_0 T_0}{c_{p0}}, \qquad \left(\frac{\partial T}{\partial p}\right)_0 = \frac{\beta_0 T_0}{\rho_0 c_{p0}}, \qquad \left(\frac{\partial T}{\partial s}\right)_0 = \frac{T_0}{c_{p0}}. \tag{2.12}$$

For ideal gases, $\beta_0 = 1/T_0$. Henceforth dropping the subscript 0 in c_0 and c_{p0}, the equations become,

$$\rho' = \frac{1}{c^2} p' - \frac{\rho_0}{c_p} s', \tag{2.13}$$

$$T' = \frac{1}{\rho_0 c_p} p' + \frac{T_0}{c_p} s'. \tag{2.14}$$

Substituting (2.13) and (2.14) into the LHS of (2.9),

$$\text{LHS} = \frac{\partial}{\partial t}\left(\frac{1}{2}\rho_0 v'^2\right) + \frac{\partial}{\partial t}\left(\frac{1}{2}\frac{1}{c^2 \rho_0} p'^2\right) + \frac{\partial}{\partial t}\left(\frac{1}{2}\frac{\rho_0 T_0}{c_p} s'^2\right). \tag{2.15}$$

The third and forth term on the RHS of (2.9) can be written as,

$$\boldsymbol{v}' \cdot (\nabla \cdot \boldsymbol{\tau}') = \nabla \cdot (\boldsymbol{\tau}' \cdot \boldsymbol{v}') - \boldsymbol{\tau}' : \nabla \boldsymbol{v}', \tag{2.16}$$

$$\begin{aligned} \frac{T'}{T_0} k \nabla^2 T' &= \nabla \cdot \left(\frac{T'}{T_0} k \nabla T'\right) - \nabla T' \cdot \nabla k \frac{T'}{T_0} \\ &= \nabla \cdot \left(\frac{T'}{T_0} k \nabla T'\right) - k \frac{(\nabla T')^2}{T_0} + k \frac{T'}{T_0^2} \nabla T_0 \cdot \nabla T'. \end{aligned} \tag{2.17}$$

Since $\nabla p_0 = 0$, it is easy to show that

$$-\frac{1}{\rho_0}\nabla \rho_0 = \frac{1}{T_0}\nabla T_0 = \frac{1}{c_p}\nabla s_0. \tag{2.18}$$

Substituting the above equation and rearranging,

$$\begin{aligned}\mathrm{RHS} = & -\nabla\cdot\left(p'\boldsymbol{v}' - \boldsymbol{\tau}'\cdot\boldsymbol{v}' - \frac{T'}{T_0}k\nabla T'\right) + \left(p' - \rho_0 c_p T'\right)\boldsymbol{v}'\cdot\frac{\nabla T_0}{T_0} \\ & + \frac{T'}{T_0}k\nabla T'\cdot\frac{\nabla T_0}{T_0} - \left(\boldsymbol{\tau}' : \nabla\boldsymbol{v}' + k\frac{(\nabla T')^2}{T_0}\right). \end{aligned} \tag{2.19}$$

In a similar manner as in (2.10)–(2.14), thermodynamic relation $s = s(T, p)$ becomes,

$$s' = \frac{c_p}{T_0}T' - \frac{1}{T_0\rho_0}p'. \tag{2.20}$$

After substituting the above equation into (2.19) and rearranging, (2.9) can be written as,

$$\frac{\partial w}{\partial t} + \nabla\cdot I = -\mathcal{D}_\nu - \mathcal{D}_k + \mathcal{P}, \tag{2.21}$$

where,

$$w = \frac{1}{2}\rho_0 v'^2 + \frac{1}{2}\frac{1}{c^2\rho_0}p'^2 + \frac{1}{2}\frac{\rho_0 T_0}{c_p}s'^2, \tag{2.22}$$

$$I = p'\boldsymbol{v}' - \boldsymbol{\tau}'\cdot\boldsymbol{v}' - \frac{T'}{T_0}k\nabla T', \tag{2.23}$$

$$\mathcal{D}_\nu = \boldsymbol{\tau}' : \nabla\boldsymbol{v}', \tag{2.24}$$

$$\mathcal{D}_k = k\frac{(\nabla T')^2}{T_0}, \tag{2.25}$$

$$\mathcal{P} = \left(\frac{T'}{T_0}k\nabla T' - T_0\rho_0 s'\boldsymbol{v}'\right)\frac{\nabla T_0}{T_0}. \tag{2.26}$$

The disturbance energy corollary (2.21) is a central contribution of the present work; it describes the disturbance energy conservation law obtained from the linearised governing equations. The term $\frac{\partial w}{\partial t}$ is the time rate of change of disturbance energy per unit volume in a infinitesimal control volume. The term I represents the energy transported per unit area and time on the surfaces of the infinitesimal control volume due to the fluctuation of pressure, velocity and temperature. The transport is due to the flow work ($p'\boldsymbol{v}'$), the work done by viscous stresses ($\boldsymbol{\tau}'\cdot\boldsymbol{v}'$) and the heat conduction ($\frac{T'}{T_0}k\nabla T'$). The term I is a more general representation of the energy flux transported by waves than the commonly used acoustic energy flux or acoustic intensity (namely fluctuating flow work $p'\boldsymbol{v}'$). Hence I is referred to as *disturbance energy flux* in this study to reflect this generalization, but 'acoustic energy' is still casually used to resonate with readers. A positive $\nabla\cdot I$ means more disturbance energy flows out of the control volume than what flows in; hence there is a spatial increase of energy transported by the waves. In other words, there is wave growth. Similarly, a negative $\nabla\cdot I$ means a spatial decrease of wave energy, i.e. wave decay. Practically, there are two types of thermoacoustic device depending on the sign of $\nabla\cdot I$. The positive $\nabla\cdot I$ is the desirable output of a thermoacoustic engine, in which case the wave is amplified; the negative $\nabla\cdot I$ is the energy input to thermoacoustic refrigerators where acoustic energy is consumed.

The non-negative $\mathcal{D}_\nu$ and $\mathcal{D}_k$ are analogous to the ordinary viscous dissipation function and irreversible heat conduction dissipation but here solely result from the gradients of fluctuating velocity and temperature. For brevity, they are referred to here as viscous and thermal dissipation, respectively.

The final term $\mathcal{P}$ in equation (2.21) contains fluctuating heat conduction ($\frac{T'}{T_0}k\nabla T'$),

energy contained in the fluctuating entropy transportation $-T_0\rho_0 s'\boldsymbol{v}'$ and temperature gradient ($\frac{\nabla T}{T}$). This newly proposed term $\mathcal{P}$ reveals the role of ∇T_0 as a disturbance energy source or sink in thermoacoustic devices. To better explain this, assume that the disturbances are periodic and then take the time average over one period, $\bar{f} = \frac{1}{T}\int_{t_0}^{t_0+T} f\,\mathrm{d}t$, where f is an arbitrary scaler. It follows that $\overline{\frac{\partial f}{\partial t}} = 0$. Taking the time average on both sides of equation (2.21) leads to $\overline{\frac{\partial w}{\partial t}} = 0$ and hence,

$$\nabla \cdot \bar{I} = -\overline{\mathcal{D}_\nu} - \overline{\mathcal{D}_k} + \overline{\mathcal{P}}, \tag{2.27}$$

which is the time-averaged disturbance energy corollary. The following of this paper discusses only the cycled-averaged effects as opposed to instantaneous changes; for clarity, equation (2.27) is referred to as disturbance energy balance relation.

For a thermoacoustic engines, the aim is to achieve wave growth by supplying a temperature gradient. Therefore $\overline{\mathcal{P}}$ must be positive and greater than the sum of dissipation terms in order to obtain a positive $\nabla \cdot \bar{I}$. The term $\overline{\mathcal{P}}$ therefore represents the thermoacoustic production mechanism of disturbance energy and ∇T_0 is the source. It is interesting that (2.27) also offers a way of finding a critical ∇T_0 when all the disturbance energy produced is exactly dissipated. Letting $\nabla \cdot \bar{I} = 0$ yields the threshold value above which the ∇T_0 has to be if any wave growth is to be achieved. When it is below the threshold, the production is not enough to overcome dissipation; the wave decays still. A trivial case occurs when $\nabla T_0 = 0$; equation (2.21) reduces to classic disturbance energy equation (see Pierce 1981, p. 516).

For a thermoacoustic refrigerator, the aim is to establish a temperature gradient by consuming acoustic energy; hence the wave decays, which means $\nabla \cdot \bar{I} < 0$. Given non-negative dissipation, $\overline{\mathcal{P}}$ must also be negative. In this case, in addition to overcoming the dissipative processes, energy is extracted from the disturbance to maintain the mean temperature gradient. The $\overline{\mathcal{P}}$ represents the thermoacoustic consumption of disturbance energy and ∇T_0 is the sink. The duality of $\overline{\mathcal{P}}$ as production or consumption in different working modes makes the term unique. Henceforth $\overline{\mathcal{P}}$ is uniformly referred to as thermoacoustic production, with the generalization that consumption is negative production.

To the authors' knowledge, this is the first explicit mathematical identification of disturbance energy production and consumption in thermoacoustic devices. Mean temperature gradient is essential for thermoacoustic engines to operate; through the production term, its role has now been explained. By the concept of disturbance energy balance, the key engineering indicators of actual devices such as engine power output, losses, heat input are formally mapped to each term in the overarching equation.

In terms of the understanding disturbance energy conservation in general, equation (2.21) can be viewed as an extension to classic acoustic and disturbance energy equations (Pierce 1981) but also a special case of generalized disturbed flow (Chu 1965; Myers 1991) with zero mean flow and constant mean pressure. In the research field of combustion instabilities, the idea of acoustic source term is prevalent (see Nicoud & Poinsot 2005), referred to as Rayleigh criterion. Equation (2.27) can therefore be interpreted as the Rayleigh criterion for thermoacoustic devices. Finally, the disturbance energy corollary has been discussed previously under specific physical conditions including one-dimensional, inviscid, non-heat-conducting flow with mean temperature gradient (Karimi *et al.* 2008) and two-dimensional premixed laminar propane-air flame (Giauque *et al.* 2006) in a duct. In the light of relevant work, the contribution of equation (2.21) and (2.27) is the expression of the disturbance energy corollary in channels of very small aspect ratio $\varepsilon \sim O(0.01)$, with significant viscous effects, non-zero mean temperature gradient and significant heat transfer with the wall. Hence the disturbance energy balance

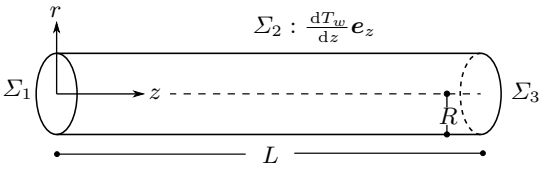

FIGURE 2. Illustration of the cylindrical control volume considered in this work. The control surfaces are labelled Σ_1 and Σ_3 for two end surfaces and Σ_2 for the curved surface. The cylindrical coordinates are established at the centre of Σ_1. Σ_2 represents the solid wall where heat transfer happens and on the wall a temperature gradient in the axial direction is applied. Σ_1 is referred to as inlet and Σ_3 as outlet.

exhibits unique features, namely, strong viscous and thermal dissipation, duality of $\overline{\mathcal{P}}$ (disturbance energy production or consumption) and $\nabla \cdot \overline{I}$ (disturbance growth or decay) and dual direction of the equations (causality), which are all linked to operating mode of thermoacoustic devices.

3. Simplification and Solution

In order to implement the analytical framework which has been established in the previous section, a particular geometry is needed. A single regenerator channel is considered here, modelled as a cylinder of radius R and length L as shown in figure 2. This shape is chosen based on the frequent use of honeycomb and stacked mesh screens in the experiments. The cylinder models the tube-like structure and has better analytical properties than a square or hexagon. In practical terms, the circular shape avoids stress concentration and abrupt changes of heat transfer around the solid wall. As shown in figure 2, an axial temperature gradient $\frac{dT_w}{dz}\mathbf{e}_z$ is imposed on the curved surface Σ_2 which represents the wall.

To speed up the computation, two set of assumptions are made to further simplify the problem: axisymmetric 2D flow and Rott's assumptions. The former is a reasonable assumption in cylindrical flow when the tangential change is negligible and the latter is a well-tested theory for thermoacoustic devices. Therefore the assumptions should incur minimal compromise on the physical understanding sought in this paper. Rott's assumptions are reviewed in the following section.

Finally, the solutions and numerical scheme are given. A global relative error was defined to test and ensure the accuracy of the numerical procedures and assumptions applied.

3.1. *Axisymmetric 2D flow assumption*

Two dimensional flow condition sets $v_\theta = 0$ and axisymmetry sets $\frac{\partial f}{\partial \theta} = 0$ where f is any scalar flow quantity or component of a vector. In cylindrical coordinates, the velocity gradient tensor reduces to,

$$\nabla \boldsymbol{v}' = \begin{bmatrix} \frac{\partial v_r'}{\partial r} & 0 & \frac{\partial v_z'}{\partial r} \\ 0 & \frac{v_r'}{r} & 0 \\ \frac{\partial v_r'}{\partial z} & 0 & \frac{\partial v_z'}{\partial z} \end{bmatrix}. \tag{3.1}$$

Note that the gradient $(\nabla \boldsymbol{v}')_{\theta\theta}$ is not zero because of the rotation of radial unit vector in $\mathbf{e}_\theta \frac{1}{r}\frac{\partial}{\partial \theta}(v_r \mathbf{e}_r)$, although $\frac{\partial v_r}{\partial \theta} = 0$. Accordingly the viscous stress tensor, applying Stokes'

hypothesis, is

$$\boldsymbol{\tau}' = \mu\left(\nabla\boldsymbol{v}' + (\nabla\boldsymbol{v}')^T\right) - \frac{2}{3}\mu(\nabla\cdot\boldsymbol{v}')\boldsymbol{I}$$
$$= \mu\begin{bmatrix} \frac{4}{3}\frac{\partial v_r'}{\partial r} - \frac{2}{3}\frac{v_r'}{r} - \frac{2}{3}\frac{\partial v_z'}{\partial z} & 0 & \frac{\partial v_z'}{\partial r} + \frac{\partial v_r'}{\partial z} \\ 0 & \frac{4}{3}\frac{v_r'}{r} - \frac{2}{3}\frac{\partial v_r'}{\partial r} - \frac{2}{3}\frac{\partial v_z'}{\partial z} & 0 \\ \frac{\partial v_z'}{\partial r} + \frac{\partial v_r'}{\partial z} & 0 & \frac{4}{3}\frac{\partial v_z'}{\partial z} - \frac{2}{3}\frac{1}{r}\frac{\partial(rv_r')}{\partial r} \end{bmatrix}. \quad (3.2)$$

Hence the acoustic viscous dissipation function $\mathcal{D}_\nu$ identified in (2.21) takes the reduced form of,

$$\mathcal{D}_\nu = \boldsymbol{\tau}' : \nabla\boldsymbol{v}'$$
$$= 2\mu\left[\left(\frac{\partial v_r'}{\partial r}\right)^2 + \left(\frac{v_r'}{r}\right)^2 + \left(\frac{\partial v_z'}{\partial z}\right)^2 + \frac{1}{2}\left(\frac{\partial v_z'}{\partial r} + \frac{\partial v_r'}{\partial z}\right)^2 - \frac{1}{3}\left(\frac{1}{r}\frac{\partial(rv_r')}{\partial r} + \frac{\partial v_z'}{\partial z}\right)^2\right]. \quad (3.3)$$

This concludes all the simplification obtained with axisymmetric cylindrical assumption.

3.2. *Rott's Assumption*

Rott (1969) has proposed three key assumptions to further simplify the linearised governing equations (2.6)–(2.8). The first two assumptions can be mathematically summarised as

$$\frac{\partial p'}{\partial r} = 0, \quad (3.4)$$

and

$$\frac{\partial T_0}{\partial r} = 0. \quad (3.5)$$

The third one, 'axial heat conduction in the acoustic wave and friction due to axial gradients are ignored', is more subtle. The first part states that heat conduction happens in the radial direction only,

$$q' = k\nabla T' = k\frac{\partial T'}{\partial r}\mathbf{e}_r, \quad (3.6)$$

and the second part states that the friction terms with $\frac{\partial}{\partial z}$ are ignored, as indicated by the inclined cross line,

$$(\nabla\cdot\boldsymbol{\tau}')\cdot\mathbf{e}_z = \mu[\underbrace{\frac{\partial^2 v_z'}{\partial r^2} + \cancel{\frac{\partial^2 v_r'}{\partial r\partial z}}}_{\frac{\partial\tau_{rz}'}{\partial r}} + \underbrace{\frac{1}{r}\frac{\partial v_z'}{\partial r} + \cancel{\frac{1}{r}\frac{\partial v_r'}{\partial z}}}_{\frac{\tau_{rz}'}{r}} + \underbrace{\cancel{\frac{1}{\partial z}\left(\frac{4}{3}\frac{\partial v_z'}{\partial z} - \frac{2}{3}\frac{1}{r}\frac{\partial(rv_r')}{\partial r}\right)}}_{\frac{\partial\tau_{zz}'}{\partial z}}]. \quad (3.7)$$

Despite its simplicity, Rott's theory has proved to be in good agreement with experimental data when linear approximation holds (see Backhaus & Swift 2000; Wu *et al.* 2014). Therefore these underlying assumptions were used in the present study to simplify (2.6)–(2.8) and this yields,

$$\frac{\partial\rho'}{\partial t} + v_z'\frac{\mathrm{d}\rho_0}{\mathrm{d}z} + \rho_0\frac{\partial v_z'}{\partial z} + \rho_0\frac{1}{r}\frac{\partial(rv_r')}{\partial r} = 0, \quad (3.8)$$

$$\rho_0\frac{\partial v_z'}{\partial t} = -\frac{\partial p'}{\partial z} + \mu\frac{\partial^2 v_z'}{\partial r^2} + \mu\frac{1}{r}\frac{\partial v_z'}{\partial r}, \quad (3.9)$$

$$\rho_0 T_0 \frac{\partial s'}{\partial t} + \rho_0 T_0 v_z' \frac{\mathrm{d}s_0}{\mathrm{d}z} = k \frac{\partial^2 T'}{\partial r^2} + k \frac{1}{r} \frac{\partial T'}{\partial r}, \tag{3.10}$$

which in this study are subject to the following boundary conditions,

$$T_0(R,z) = T_w(z), \quad T'(R,z) = 0, \quad \boldsymbol{v}'(R,z) = 0, \quad v_r'(0,z) = 0, \quad \forall z \in [0,L], \tag{3.11}$$

where function $T_w(z)$ is given. The momentum equation in the radial direction is reduced to $\frac{\partial p'}{\partial r} = 0$ and mean temperature

$$T_0(r,z) = T_w(z). \tag{3.12}$$

This concludes the simplification obtained with Rott's assumptions.

3.3. *Dimensional Analysis*

To further simplify the disturbance energy equation (2.27) and reduce the number of independent parameters, the problem is non-dimensionalised. Scaling procedures follow the ones used by In't Panhuis *et al.* (2009). The dimensionless variables, denoted by upper asterisk, are,

$$\begin{aligned}
&r = Rr^*, \qquad z = Lz^*, \qquad t = \frac{1}{\omega} t^*, \qquad v_z' = c_{\mathrm{ref}} v_z'^*, \qquad v_r' = \varepsilon c_{\mathrm{ref}} v_r'^*, \\
&\rho' = \rho_{\mathrm{ref}} \rho'^*, \quad \rho_0 = \rho_{\mathrm{ref}} \rho_0^*, \quad p' = \rho_{\mathrm{ref}} c_{\mathrm{ref}}^2 p'^*, \quad p_0 = \rho_{\mathrm{ref}} c_{\mathrm{ref}}^2 p_0^*, \quad T' = \frac{c_{\mathrm{ref}}^2}{c_p} T'^*, \\
&T_0 = \frac{c_{\mathrm{ref}}^2}{c_p} T_0^*, \quad s = c_p s'^*, \qquad s_0 = c_p s_0^*, \qquad \mu = \mu_{\mathrm{ref}} \mu^*, \qquad k = k_{\mathrm{ref}} k^*,
\end{aligned} \tag{3.13}$$

where $\varepsilon = \frac{R}{L}$ is the aspect ratio and the reference point for ρ_{ref}, c_{ref}, μ_{ref} and k_{ref} was set at the mid-point ($z_{\mathrm{ref}} = \frac{L}{2}$) of the regenerator. The governing equations in dimensionless form are,

$$He \frac{\partial \rho'^*}{\partial t^*} + v_z'^* \frac{\mathrm{d}\rho_0^*}{\mathrm{d}z^*} + \rho_0^* \frac{\partial v_z'^*}{\partial z^*} + \rho_0^* \frac{1}{r^*} \frac{\partial (r^* v_r'^*)}{\partial r^*} = 0, \tag{3.14}$$

$$\rho_0^* \frac{\partial v_z'^*}{\partial t^*} = -\frac{1}{He} \frac{\partial p'^*}{\partial z^*} + \frac{1}{Wo^2} \mu^* \left(\frac{\partial^2 v_z'^*}{\partial r^{*2}} + \frac{1}{r^*} \frac{\partial v_z'^*}{\partial r^*} \right), \tag{3.15}$$

$$\rho_0^* T_0^* \frac{\partial s'^*}{\partial t^*} + \frac{1}{He} \rho_0^* T_0^* v_z'^* \frac{\mathrm{d}s_0^*}{\mathrm{d}z^*} = \frac{1}{Pr \cdot Wo^2} \frac{k\omega}{p_0} \left(\frac{\partial^2 T'^*}{\partial r^{*2}} + \frac{1}{r^*} \frac{\partial T'^*}{\partial r^*} \right), \tag{3.16}$$

where

$$He = \frac{\omega L}{c_{\mathrm{ref}}}, \quad Wo = R \left(\frac{\omega \rho_{\mathrm{ref}}}{\mu_{\mathrm{ref}}} \right)^{\frac{1}{2}}, \tag{3.17}$$

are the Helmholtz number and the Womersley number, respectively, with Pr being the Prandtl number .

Wo^2 is the ratio of transient inertial force ($\rho_{\mathrm{ref}} \frac{c_{\mathrm{ref}}}{\frac{1}{\omega}}$) to viscous force $\mu_{\mathrm{ref}} \frac{c_{\mathrm{ref}}}{R} \frac{1}{R}$. In fact Wo^2 is also the Reynolds number when the length and time scale, instead of velocity scale, are imposed (which leads to the Strouhal number $St = 1$), namely

$$Wo^2 = Re = \frac{\rho_{\mathrm{ref}} (\omega R) R}{\mu_{\mathrm{ref}}}. \tag{3.18}$$

Correspondingly, the $Pr \cdot Wo^2$ would be Péclet number, i.e.

$$Pr \cdot Wo^2 = \frac{c_p \mu_{\mathrm{ref}}}{k_{\mathrm{ref}}} \frac{\rho_{\mathrm{ref}} (\omega R) R}{\mu_{\mathrm{ref}}} = Pe. \tag{3.19}$$

Some authors (e.g. Worlikar & Knio 1996) prefer the notion of Re and Pe but in this paper Wo^2 is used because its physical meaning can be interpreted in various ways. Firstly, Wo^2 and $Pr \cdot Wo^2$ can be interpreted as the ratio of two distances,

$$Wo = \sqrt{2}\frac{R}{\delta_\nu}, \quad \sqrt{Pr} \cdot Wo = \sqrt{2}\frac{R}{\delta_k}, \tag{3.20}$$

where

$$\delta_\nu = \sqrt{\frac{2\mu}{\omega\rho_0}}, \quad \delta_k = \sqrt{\frac{2k}{\omega\rho_0 c_p}}, \tag{3.21}$$

are the depth of Stokes layer and its thermal counterpart, respectively. They are the characteristic length of momentum and thermal diffusion in one period. Therefore if $Wo \sim O(1)$ the whole channel is filled with oscillatory boundary layer as in case of regenerators considered here and $Wo \gg 1$ are found in ordinary acoustic resonators.

Another interpretation of Wo^2 is proposed by Tominaga (1995), as the ratio of two time scales,

$$Wo^2 = \omega t_\nu, \quad Pr \cdot Wo^2 = \omega t_k, \tag{3.22}$$

and

$$t_\nu = \frac{R^2}{\nu}, \quad t_k = \frac{R^2}{\alpha}, \tag{3.23}$$

where ν is kinematic viscosity and α the thermal diffusivity while t_ν and t_k characterize the time of momentum and thermal diffusion across the channel area. Therefore Wo^2 is the time-scale of the diffusion measured in the period of oscillation.

3.3.1. *Simplification of disturbance energy terms*

In the following, the scales obtained form dimensional analysis are used to achieve the simplification of disturbance energy terms. First consider the velocity gradients,

$$\begin{array}{cccccc} & \dfrac{\partial v_r'}{\partial z} & \dfrac{\partial v_r'}{\partial r} & \dfrac{v_r'}{r} & \dfrac{\partial v_z'}{\partial z} & \dfrac{\partial v_z'}{\partial r}. \\ \dfrac{c_{\mathrm{ref}}}{L}\cdot & (\ \varepsilon & 1 & 1 & 1 & \dfrac{1}{\varepsilon}\ ) \end{array} \tag{3.24}$$

The scales are written beneath as the product of a common factor (in this case $\frac{c_{\mathrm{ref}}}{L}$) and relative orders defined as ε^2, ε, 1, $1/\varepsilon$, $1/\varepsilon^2$. Note that the aspect ratio ε is small, $\varepsilon \sim O(0.01)$.

The rationale behind the Rott's third assumption, namely equation (3.6) and (3.7), becomes clearer with this dimensional analysis, because,

$$\begin{array}{l} (\nabla \cdot \boldsymbol{\tau}') \cdot \mathbf{e}_z = \mu \left[\dfrac{\partial^2 v_z'}{\partial r^2} + \dfrac{\partial^2 v_r'}{\partial r \partial z} + \dfrac{1}{r}\dfrac{\partial v_z'}{\partial r} + \dfrac{1}{r}\dfrac{\partial v_r'}{\partial z} + \dfrac{1}{\partial z}\left(\dfrac{4}{3}\dfrac{\partial v_z'}{\partial z} - \dfrac{2}{3}\dfrac{1}{r}\dfrac{\partial (r v_r')}{\partial r} \right) \right], \\ \dfrac{\mu_{\mathrm{ref}} c_{\mathrm{ref}}}{L^2}\cdot \quad \left(\dfrac{1}{\varepsilon^2} \quad 1 \quad \dfrac{1}{\varepsilon^2} \quad 1 \quad 1 \right). \end{array} \tag{3.25}$$

The leading terms $\frac{\partial^2 v_z'}{\partial r^2}$ and $\frac{1}{r}\frac{\partial v_z'}{\partial r}$, which are kept in the assumption, are two orders larger than the rest. Similarly,

$$\begin{array}{l} \mathbf{q}' = k\left(\dfrac{\partial T'}{\partial r}\mathbf{e}_r + \dfrac{\partial T'}{\partial z}\mathbf{e}_z \right), \\ \dfrac{k_{\mathrm{ref}} T_{\mathrm{ref}}}{L}\cdot \quad \left(\dfrac{1}{\varepsilon} \quad 1 \right). \end{array} \tag{3.26}$$

the radial heat flux is one order bigger than the axial heat flux.

Now apply the order of magnitude analysis to the terms in disturbance energy equation. The scales of squared terms in viscous dissipation are,

$$\left(\frac{\partial v_r'}{\partial r}\right)^2 + \left(\frac{v_r'}{r}\right)^2 + \left(\frac{\partial v_z'}{\partial z}\right)^2 + \frac{1}{2}\left(\frac{\partial v_z'}{\partial r} + \frac{\partial v_r'}{\partial z}\right)^2 - \frac{1}{3}\left(\frac{1}{r}\frac{\partial (r v_r')}{\partial r} + \frac{\partial v_z'}{\partial z}\right)^2,$$

$$\left(\frac{c_{\mathrm{ref}}}{L}\right)^2 \cdot \quad (\quad 1 \qquad 1 \qquad 1 \qquad \frac{1}{\varepsilon^2} \quad \varepsilon^2 \qquad 1 \qquad 1 \quad) \quad .$$

The leading term $(\frac{\partial v_z'}{\partial r})^2$ is two orders larger than the rest, so the viscous dissipation can be assumed to be,

$$\mathcal{D}_\nu = \mu\left(\frac{\partial v_z'}{\partial r}\right)^2, \tag{3.27}$$

without losing much accuracy.

For thermal dissipation, simply applying Rott's assumption equation (3.6), yields,

$$\mathcal{D}_k = k\frac{(\nabla T')^2}{T_0} = \frac{k}{T_0}\left(\frac{\partial T'}{\partial r}\right)^2. \tag{3.28}$$

For the production term, given that the direction of ∇T_0 as shown in figure 2 is orthogonal to the direction of simplified heat flux, it takes the form of,

$$\begin{aligned}\mathcal{P} &= \left(k\frac{T'}{T_0}\nabla T' - T_0\rho_0 s'\boldsymbol{v}'\right)\cdot\frac{\nabla T_0}{T_0}\\ &= k\frac{T'}{T_0^2}\frac{\partial T'}{\partial r}\mathbf{e}_r\frac{\mathrm{d}T_0}{\mathrm{d}z}\mathbf{e}_z - \rho_0 s' v_z'\mathbf{e}_z\frac{\mathrm{d}T_0}{\mathrm{d}z}\mathbf{e}_z - \rho_0 s' v_r'\mathbf{e}_r\frac{\mathrm{d}T_0}{\mathrm{d}z}\mathbf{e}_z\\ &= -\rho_0 s' v_z'\frac{\mathrm{d}T_0}{\mathrm{d}z}.\end{aligned} \tag{3.29}$$

Finally consider the disturbance energy flux term by term,

$$\nabla\cdot I = \nabla\cdot(p'\boldsymbol{v}') - \nabla\cdot(\boldsymbol{\tau}'\cdot\boldsymbol{v}') - \nabla\cdot(\frac{T'}{T_0}k\nabla T'). \tag{3.30}$$

With $\boldsymbol{\tau}' : \nabla\boldsymbol{v}'$ and $\boldsymbol{v}'\cdot(\nabla\cdot\boldsymbol{\tau}')$ already individually simplified, given the divergence identity, it must satisfy

$$\begin{aligned}\nabla\cdot(\boldsymbol{\tau}'\cdot\boldsymbol{v}') &= \boldsymbol{v}'\cdot(\nabla\cdot\boldsymbol{\tau}') + \boldsymbol{\tau}' : \nabla\boldsymbol{v}'\\ &= \mu[v_z\frac{\partial^2 v_z}{\partial r^2} + v_z\frac{1}{r}\frac{\partial v_z'}{\partial r} + \left(\frac{\partial v_z'}{\partial r}\right)^2].\end{aligned} \tag{3.31}$$

From the simplified form of $\nabla\cdot(\boldsymbol{\tau}'\cdot\boldsymbol{v}')$, $\boldsymbol{\tau}' : \nabla\boldsymbol{v}'$ and $\boldsymbol{v}'\cdot(\nabla\cdot\boldsymbol{\tau}')$, an *equivalent* stress tensor can be defined as,

$$\boldsymbol{\tau}_e' = \begin{bmatrix}0 & 0 & \tau_{rz}\\ 0 & 0 & 0\\ 0 & 0 & 0\end{bmatrix} = \mu\begin{bmatrix}0 & 0 & \frac{\partial v_z'}{\partial r}\\ 0 & 0 & 0\\ 0 & 0 & 0\end{bmatrix}. \tag{3.32}$$

Note that the stress tensor is said to be 'equivalent' because it leads to the correct simplified form (3.7), (3.27), (3.31) but it does not obey symmetry and Stokes' hypothesis. The equivalent tensor is useful in determining $\boldsymbol{\tau}'\cdot\boldsymbol{v}'$ in the following paragraphs.

Similarly,

$$\nabla \cdot (\frac{T'}{T_0} k \nabla T') = \frac{T'}{T_0} k \nabla^2 T' + k \frac{(\nabla T')^2}{T_0} - k \frac{T'}{T_0^2} \nabla T_0 \cdot \nabla T' = \frac{T'}{T_0} k \left(\frac{\partial^2 T'}{\partial r^2} + \frac{1}{r} \frac{\partial T'}{\partial r} \right) + \frac{1}{T_0} k \left(\frac{\partial T'}{\partial r} \right)^2 . \tag{3.33}$$

Taking advantage of the boundary conditions, $\nabla \cdot I$ can be further simplified in the integral form. The control volume in this study was a cylinder bounded by three surfaces Σ_1, Σ_2 and Σ_3 as shown in figure 2. Integrating the time-averaged disturbance energy balance relation (2.27) over it and applying Green's theorem, yields

$$\iint_{\Sigma} \mathbf{n} \cdot \overline{I} \, \mathrm{d}S = - \iiint_{\Omega} \overline{\mathcal{D}_\nu} \, \mathrm{d}V - \iiint_{\Omega} \overline{\mathcal{D}_k} \, \mathrm{d}V + \iiint_{\Omega} \overline{\mathcal{P}} \, \mathrm{d}V, \tag{3.34}$$

where $\mathbf{n}$ is the outward-pointing unit normal vector on Σ. Equation (3.34) is the integral form of time-averaged disturbance energy balance relation.

The instantaneous disturbance energy flux is,

$$\iint_{\Sigma} \mathbf{n} \cdot I \, \mathrm{d}S = \iint_{\Sigma} \mathbf{n} \cdot (p' \boldsymbol{v}' - \boldsymbol{\tau}' \cdot \boldsymbol{v}' - \frac{T'}{T_0} k \nabla T') \, \mathrm{d}S. \tag{3.35}$$

On Σ_2, the boundary conditions (3.11) sets the integration (3.35) to zero and on Σ_1 and Σ_3, $\mathbf{n}$ was parallel to $\mathbf{e}_z$, so (3.35) becomes,

$$\iint_{\Sigma} \mathbf{n} \cdot I \, \mathrm{d}S = \iint_{\Sigma_3} \mathbf{e}_z \cdot (p' \boldsymbol{v}' - \boldsymbol{\tau}' \cdot \boldsymbol{v}' - \frac{T'}{T_0} k \nabla T') \, \mathrm{d}S - \iint_{\Sigma_1} \mathbf{e}_z \cdot (p' \boldsymbol{v}' - \boldsymbol{\tau}' \cdot \boldsymbol{v}' - \frac{T'}{T_0} k \nabla T') \, \mathrm{d}S. \tag{3.36}$$

With the equivalent stress tensor already defined, it is found that

$$\boldsymbol{\tau}' \cdot \boldsymbol{v}' = \boldsymbol{\tau}_e' \cdot \boldsymbol{v}' = \tau_{rz}' v_z' \mathbf{e}_r = \mu \frac{\partial v_z'}{\partial r} v_z' \mathbf{e}_r, \tag{3.37}$$

$$\frac{T'}{T_0} k \nabla T' = \frac{T'}{T_0} k \frac{\partial T'}{\partial r} \mathbf{e}_r, \tag{3.38}$$

which are both orthogonal to $\mathbf{e}_z$.

Hence the final simplified expression of $\iint_{\Sigma} \mathbf{n} \cdot I \, \mathrm{d}S$ in a cylindrical domain is,

$$\iint_{\Sigma} \mathbf{n} \cdot I \, \mathrm{d}S = \iint_{\Sigma_3} p' v_z' \, \mathrm{d}S - \iint_{\Sigma_1} p' v_z' \, \mathrm{d}S. \tag{3.39}$$

Therefore it is shown that, after the simplification, the disturbance energy flux in a cylindrical domain reduces to the classic acoustic flux.

This section has reported in detail the simplification of $\mathcal{D}_\nu$, $\mathcal{D}_k$, $\mathcal{P}$ and $\iint \mathbf{n} \cdot I \, \mathrm{d}S$, taking the form of (3.27), (3.28), (3.29) and (3.39), respectively.

3.3.2. *Dimensionless disturbance energy balance*

The integral form of the disturbance energy balance is non-dimensionalised using integrated inlet disturbance energy flux $(\mathbf{n} \cdot \overline{I})_{\Sigma_1}$. Shorthand notation $(\cdot)_{\mathrm{cv}}$ and $(\cdot)_{\mathrm{cs}}$

are used for $\iiint_{\Omega} \cdot \mathrm{d}V$ and $\iint_{\Sigma} \cdot \mathrm{d}S$, respectively. The equation takes the form of,

$$(\mathbf{n} \cdot \overline{I})^*_{\mathrm{cs}} = -(\overline{\mathcal{D}_\nu})^*_{\mathrm{cv}} - (\overline{\mathcal{D}_k})^*_{\mathrm{cv}} + (\overline{\mathcal{P}})^*_{\mathrm{cv}}, \tag{3.40}$$

where each term

$$(\cdot)^*_{\mathrm{cs|cv}} = \frac{(\cdot)_{\mathrm{cs|cv}}}{(\mathbf{n} \cdot \overline{I})_{\Sigma_1}}. \tag{3.41}$$

The $(\mathbf{n} \cdot \overline{I})^*_{\mathrm{cs}}$ then represents the relative wave growth; $(\overline{\mathcal{P}})^*$, $(\overline{\mathcal{D}_\nu})^*$, $(\overline{\mathcal{D}_k})^*$ are production, viscous dissipation and thermal dissipation relative to the energy transported by the wave, respectively. The benefit of scaling in this way is to offer better intuition since terms are expressed as fractions or multiples of inlet energy and are hence $O(1)$. Also the equality of left and right side of the equation can be easily shown by taking the difference $\Delta^* = (\overline{\mathcal{P}})^*_{\mathrm{cv}} - (\overline{\mathcal{D}_\nu})^*_{\mathrm{cv}} - (\overline{\mathcal{D}_\nu})^*_{\mathrm{cv}} - (\mathbf{n} \cdot \overline{I})^*_{\mathrm{cs}}$.

It is worth noting that another possible scaling procedures is to non-dimensionalise the energy terms by its respective flow variables. For example,

$$(\overline{\mathcal{D}_k})_{\mathrm{cv}} = \int_0^L \int_0^R \frac{k}{T_0} \left(\frac{\partial T'}{\partial r}\right)^2 r \,\mathrm{d}r \,\mathrm{d}l = k_{\mathrm{ref}} T_{\mathrm{ref}} L \int_0^1 \int_0^1 \frac{k^*}{T_0^*} \left(\frac{\partial T'^*}{\partial r^*}\right)^2 r^* \,\mathrm{d}r^* \,\mathrm{d}l^* \tag{3.42}$$

Define,

$$(\overline{\mathcal{D}_k})^\dagger = \frac{k^*}{T_0^*} \left(\frac{\partial T'^*}{\partial r^*}\right)^2, \qquad (\overline{\mathcal{D}_k})^\dagger_{\mathrm{cv}} = \int_0^1 \int_0^1 (\overline{\mathcal{D}_k})^\dagger r^* \,\mathrm{d}r^* \,\mathrm{d}l^*, \tag{3.43}$$

where the dagger (†) superscript denotes non-dimensionalisation using corresponding flow variables. It can be shown that the two non-dimensionalisation methods are equivalent because,

$$(\overline{\mathcal{D}_k})^*_{\mathrm{cv}} = \frac{(\overline{\mathcal{D}_k})_{\mathrm{cv}}}{(\mathbf{n} \cdot \overline{I})_{\Sigma_1}} = \frac{k_{\mathrm{ref}} \frac{c_{\mathrm{ref}}^2}{c_p} L (\overline{\mathcal{D}_k})^\dagger}{\rho_{\mathrm{ref}} c_{\mathrm{ref}}^3 R^2 (\mathbf{n} \cdot \overline{I})^\dagger_{\Sigma_1}} = \frac{He}{Wo^2} \frac{(\overline{\mathcal{D}_k})^\dagger}{(\mathbf{n} \cdot \overline{I})^\dagger_{\Sigma_1}}. \tag{3.44}$$

For two dynamically similar flows, He, Wo^2, $(\overline{\mathcal{D}_k})^\dagger$, $(\mathbf{n} \cdot \overline{I})^\dagger_{\Sigma_1}$ are identical and hence so are $(\overline{\mathcal{D}_k})^*_{\mathrm{cv}}$. Similarly,

$$(\overline{\mathcal{D}_\nu})^\dagger = \mu^* \left(\frac{\partial v_z'^*}{\partial r^*}\right)^2, \qquad (\overline{\mathcal{D}_\nu})^\dagger_{\mathrm{cv}} = \int_0^1 \int_0^1 (\overline{\mathcal{D}_\nu})^\dagger r^* \,\mathrm{d}r^* \,\mathrm{d}l^*. \tag{3.45}$$

$$(\overline{\mathcal{P}})^\dagger = -\rho_0^* s'^* v_z'^* \frac{\mathrm{d}T_0^*}{\mathrm{d}z^*}, \qquad (\overline{\mathcal{P}})^\dagger_{\mathrm{cv}} = \int_0^1 \int_0^1 (\overline{\mathcal{P}})^\dagger r^* \,\mathrm{d}r^* \,\mathrm{d}l^*. \tag{3.46}$$

The equivalence of these two methods allows us to use the flow variables and equation (3.43), (3.45) and (3.46) to explain the trends of disturbance energy terms defined in (3.40).

The differential disturbance energy balance is non-dimensionalised using inlet flux density $(\nabla \cdot \overline{I})_{\Sigma_1}$ on the axis $r = 0$,

$$(\nabla \cdot \overline{I})^* = -(\overline{\mathcal{D}_\nu})^* - (\overline{\mathcal{D}_k})^* + (\overline{\mathcal{P}})^*, \tag{3.47}$$

where each term

$$(\cdot)^* = \frac{(\cdot)}{(\nabla \cdot \overline{I})_{\Sigma_1, r=0}}. \tag{3.48}$$

This section has shown the non-dimensionalisation of the governing equations. It has also discussed key dimensionless groups: He and Wo, the simplification of disturbance energy terms and the non-dimensionalisation of the disturbance energy balance.

3.4. *Solution*

Assuming that all the disturbances are time-harmonic signals with angular frequency ω, equation (3.8)–(3.10) can be solved in the frequency domain $f'(\mathbf{x},t) = \mathrm{Re}(\hat{f}(\mathbf{x})e^{\mathrm{i}\omega t})$ where $\hat{f}(\mathbf{x})$ is the complex amplitude. Since instantaneous values are of no interests in this study, no distinction is made between frequency-domain and time-domain variables. Complex and real disturbance are uniformly denoted as f', whose meaning should be clear in the context. The equations were solved in two dimensions instead of using area average performed by Rott in the original paper and most of subsequent work.

Note that the solutions are given in dimensional form on purpose because it is easier for readers to compare the solutions reported here with those in the previous literature. Dimensional form is also easier to interpret in practice for implementation. Dimensionless solutions are given on an ad-hoc basis when they are needed in the results section.

Velocity and temperature fluctuation were solved in terms of p' and $\frac{\mathrm{d}p'}{\mathrm{d}z}$, with i being the complex unit,

$$v_z' = \frac{1-\mathcal{H}_\nu}{-\mathrm{i}\omega\rho_0}\frac{\mathrm{d}p'}{\mathrm{d}z}, \tag{3.49}$$

$$v_r' = \frac{1}{2}r\left[-\frac{\mathrm{i}\omega}{p_0}\frac{1+(\gamma-1)\mathcal{G}_k}{\gamma}p' + \frac{\mathrm{i}R_g}{\omega p_0}\frac{\mathrm{d}T_w}{\mathrm{d}z}\frac{\mathcal{G}_k-\mathcal{G}_\nu}{1-Pr}\frac{\mathrm{d}p'}{\mathrm{d}z} - \frac{\partial}{\partial z}\left(\frac{1-\mathcal{G}_\nu}{-\mathrm{i}\omega\rho_0}\frac{\mathrm{d}p'}{\mathrm{d}z}\right)\right], \tag{3.50}$$

$$T' = \frac{1-\mathcal{H}_k}{\rho_0 c_p}p' - \frac{1}{\rho_0\omega^2}\frac{\mathrm{d}T_w}{\mathrm{d}z}\frac{(1-\mathcal{H}_k)-Pr(1-\mathcal{H}_\nu)}{1-Pr}\frac{\mathrm{d}p'}{\mathrm{d}z}, \tag{3.51}$$

$$s' = \frac{-\mathcal{H}_k}{\rho_0 T_0}p' - \frac{c_p}{\rho_0 T_0\omega^2}\frac{\mathrm{d}T_w}{\mathrm{d}z}\frac{(1-\mathcal{H}_k)-Pr(1-\mathcal{H}_\nu)}{1-Pr}\frac{\mathrm{d}p'}{\mathrm{d}z}, \tag{3.52}$$

where the radial distribution is given by

$$\mathcal{H}(r,z) = \frac{J_0\left[(\mathrm{i}-1)\,r/\delta\right]}{J_0\left[(\mathrm{i}-1)R/\delta\right]}. \tag{3.53}$$

J_0 and J_1 are Bessel functions of the first kind of order 0 and 1, respectively. $\mathcal{H}_\nu$ uses viscous boundary layer thickness δ_ν, and $\mathcal{H}_k$ uses thermal boundary layer thickness δ_k, as defined in equation (3.21). The solution structure was adapted from Swift (2002). Notice that $\mathcal{H}$ contains R/δ_ν and R/δ_k which are the local $\frac{1}{\sqrt{2}}Wo$ and $\frac{1}{\sqrt{2}}\sqrt{Pr}\,Wo$, underlying again the importance of the Womersley number. The radial distribution function $\mathcal{G}$ is defined as the area average of $\mathcal{H}$ in a circle of radius r,

$$\mathcal{G}(r,z) = \frac{2}{r^2}\int \mathcal{H}r\,\mathrm{d}r = \frac{2\delta}{(\mathrm{i}-1)r}\frac{J_1\left[(\mathrm{i}-1)\,r/\delta\right]}{J_0\left[(\mathrm{i}-1)R/\delta\right]}. \tag{3.54}$$

which also has two form $\mathcal{G}_\nu$ and $\mathcal{G}_k$. At $r=0$,

$$\mathcal{G}(z,0) := \lim_{r\to 0^+}\mathcal{G}(r,z) = 1/J_0\left[(\mathrm{i}-1)R/\delta\right] = \mathcal{H}(z,0). \tag{3.55}$$

The derivatives needed to evaluate the simplified $\mathcal{P}$, $\mathcal{D}_\nu$, $\mathcal{D}_k$ were also derived,

$$\frac{\partial v_z'}{\partial r} = \frac{\mathcal{I}_v}{-\mathrm{i}\omega\rho_0}\frac{\mathrm{d}p'}{\mathrm{d}z}, \tag{3.56}$$

$$\frac{\partial v_z'}{\partial z} = \frac{\partial}{\partial z}\left(\frac{1-\mathcal{H}_v}{-\mathrm{i}\omega\rho_0}\frac{\mathrm{d}p'}{\mathrm{d}z}\right), \tag{3.57}$$

$$\frac{\partial v_r'}{\partial r} = -\frac{\mathrm{i}\omega}{2p_0\gamma}p' - \frac{\mathrm{i}}{2\omega}\frac{\mathrm{d}}{\mathrm{d}z}\left(\frac{1}{\rho_0}\frac{\mathrm{d}p'}{\mathrm{d}z}\right) - \frac{\mathrm{i}\omega}{p_0}\frac{(\gamma-1)\left(\mathcal{H}_k - \frac{1}{2}\mathcal{G}_k\right)}{\gamma}p' + \frac{\mathrm{i}R_g}{\omega p_0}\frac{\mathrm{d}T_w}{\mathrm{d}z}\frac{(\mathcal{H}_k - \frac{1}{2}\mathcal{G}_k) - (\mathcal{H}_\nu - \frac{1}{2}\mathcal{G}_\nu)}{1-Pr}\frac{\mathrm{d}p'}{\mathrm{d}z} - \frac{\partial}{\partial z}\left(\frac{\mathcal{H}_\nu - \frac{1}{2}\mathcal{G}_\nu}{-\mathrm{i}\omega\rho_0}\frac{\mathrm{d}p'}{\mathrm{d}z}\right), \tag{3.58}$$

$$\frac{\partial T'}{\partial r} = \frac{1}{\rho_0 c_p}\mathcal{I}_k p' - \frac{1}{\rho_0\omega^2}\frac{\mathrm{d}T_w}{\mathrm{d}z}\frac{\mathcal{I}_k - Pr\mathcal{I}_\nu}{1-Pr}\frac{\mathrm{d}p'}{\mathrm{d}z}, \tag{3.59}$$

with

$$\mathcal{I}(r,z) = -\frac{\partial\mathcal{H}}{\partial r} = \frac{\mathrm{i}-1}{\delta}\frac{J_1\left[(\mathrm{i}-1)\,r/\delta\right]}{J_0\left[(\mathrm{i}-1)R/\delta\right]}. \tag{3.60}$$

This concludes the definition of radial distribution functions $\mathcal{H}$, $\mathcal{G}$, $\mathcal{I}$ and the analytical solutions in the radial direction in terms of p' and $\frac{\mathrm{d}p'}{\mathrm{d}z}$.

3.5. *Numerical Scheme*

Since all the flow quantities were expressed in terms of p' and $\frac{\mathrm{d}p'}{\mathrm{d}z}$, it is important to find an efficient numerical scheme to solve them in the axial direction. Now let,

$$\mathcal{F}(z) = \mathcal{G}(R,z). \tag{3.61}$$

Then evaluating (3.50) at R and applying the non-slip boundary condition $v_r(R,z)=0$, yields,

$$-\frac{\mathrm{i}\omega}{p_0}\frac{1+(\gamma-1)\mathcal{F}_k}{\gamma}p' + \frac{1}{T_w}\frac{\mathrm{d}T_w}{\mathrm{d}z}\frac{\mathcal{F}_k - \mathcal{F}_\nu}{(1-\mathcal{F}_\nu)(1-Pr)}\left(\frac{1-\mathcal{F}_\nu}{-\mathrm{i}\omega\rho_0}\frac{\mathrm{d}p'}{\mathrm{d}z}\right) - \frac{\mathrm{d}}{\mathrm{d}z}\left(\frac{1-\mathcal{F}_\nu}{-\mathrm{i}\omega\rho_0}\frac{\mathrm{d}p'}{\mathrm{d}z}\right) = 0. \tag{3.62}$$

which is Rott's thermoacoustic wave equation. Function $\mathcal{F}(z)$ is the area average of $\mathcal{H}$ on the entire circular cross-section and hence (3.62) only depends on z. The physical meaning of the term $\frac{1-\mathcal{F}_\nu}{-\mathrm{i}\omega\rho_0}\frac{\mathrm{d}p'}{\mathrm{d}z}$ is area-averaged axial velocity $(v_z')_{\mathrm{av}}$ because

$$(v_z')_{\mathrm{av}} = \frac{1}{\pi R^2}\int_0^R \frac{1-\mathcal{H}_\nu}{-\mathrm{i}\omega\rho_0}\frac{\mathrm{d}p'}{\mathrm{d}z}2\pi r\,\mathrm{d}r = \frac{1-\mathcal{G}_\nu(R,z)}{-\mathrm{i}\omega\rho_0}\frac{\mathrm{d}p'}{\mathrm{d}z} = \frac{1-\mathcal{F}_\nu(z)}{-\mathrm{i}\omega\rho_0}\frac{\mathrm{d}p'}{\mathrm{d}z}. \tag{3.63}$$

Therefore the second-order ODE (3.62) can be conveniently converted to two simultaneous first-order ODEs,

$$\frac{\mathrm{d}p'}{\mathrm{d}z} = \frac{-\mathrm{i}\omega\rho_0}{1-\mathcal{F}_\nu(z)}(v_z')_{\mathrm{av}}, \tag{3.64a}$$

$$\frac{\mathrm{d}(v_z')_{\mathrm{av}}}{\mathrm{d}z} = -\frac{\mathrm{i}\omega}{p_0}\frac{1+(\gamma-1)\mathcal{F}_k}{\gamma}p' + \frac{1}{T_w}\frac{\mathrm{d}T_w}{\mathrm{d}z}\frac{\mathcal{F}_k-\mathcal{F}_\nu}{(1-\mathcal{F}_\nu)(1-Pr)}(v_z')_{\mathrm{av}}, \tag{3.64b}$$

and the use of $(v_z')_{\mathrm{av}}$ instead of $\frac{1-\mathcal{F}_\nu}{-\mathrm{i}\omega\rho_0}\frac{\mathrm{d}p'}{\mathrm{d}z}$ gives more physical intuition. Given R, ω, p_0, values of p' and $\frac{\mathrm{d}p'}{\mathrm{d}z}$ at any point, (3.62) can be solved progressively. In this study, $(v_z')_{\mathrm{av}}$ and p' were given at the inlet (Σ_1 shown in figure 2) as boundary conditions and (3.62) was solved using 8th-order Dormand-Prince method (Prince & Dormand 1981) with new embedded formulas (Hairer *et al.* 1993, p. 255). The local absolute and relative error tolerance used for the adaptive stepsize control were both 10^{-6}. The output positions were specified and then interim stepsize was automatically adjusted depending on the ratio of specified tolerance to local error. With p' and $\frac{\mathrm{d}p'}{\mathrm{d}z}$, it is very easy to obtain T' and v_z' since the solutions are radially analytical as mentioned previously. In contrast, for second-order derivatives which contain $\mathcal{H}$ or $\mathcal{G}$, such as $\frac{\partial}{\partial z}\left(\frac{1-\mathcal{G}_\nu}{-\mathrm{i}\omega\rho_0}\frac{\mathrm{d}p'}{\mathrm{d}z}\right)$ in v_r', it is technically

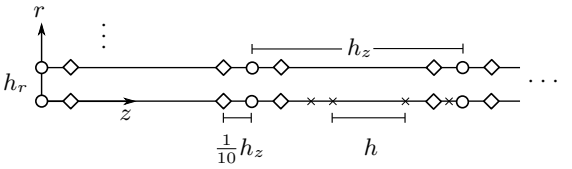

FIGURE 3. Illustration of computational grid in this study, including main output points (○), auxiliary points (◊) and interim points (×). h_z and h_r are the axial and radial output stepsize, respectively. h is the self-adaptive integration stepsize.

possible to obtain the analytical solutions but complexity is an issue, especially the implicit z dependence of δ, which is contained in $\mathcal{H}$ or $\mathcal{G}$. Therefore the central difference formula was used for the evaluating second-order derivative containing radial distribution functions. Instead of using the main output points for the central difference calculation, auxiliary points were added on both sides of the main output points, as shown in figure 3, to increase the accuracy.

A global error is needed to validate the simplification made and ensure overall accuracy of the numerical procedures. In linear regime, (3.34) holds exactly. The equality is compromised by simplification and use of numerical methods. Therefore in this study the global relative error was defined as,

$$\epsilon = \frac{|(\overline{\mathcal{P}})_{\mathrm{cv}} - (\overline{\mathcal{D}_\nu})_{\mathrm{cv}} - (\overline{\mathcal{D}_k})_{\mathrm{cv}} - (\mathbf{n}\cdot\overline{I})_{\mathrm{cs}}|}{\max(|(\overline{\mathcal{P}})_{\mathrm{cv}}|, |(\overline{\mathcal{D}_\nu})_{\mathrm{cv}}|, |(\overline{\mathcal{D}_k})_{\mathrm{cv}}|, |(\mathbf{n}\cdot\overline{I})_{\mathrm{cs}}|)}. \tag{3.65}$$

The mesh numbers were adjusted during the computation to reach a satisfactory error level (here in the order of 10^{-5}) to balance computation speed and accuracy.

4. Results and Discussion

The aim of the present study is to establish a new analytical framework to clarify the disturbance energy conservation in thermoacoustic devices. In order to demonstrate the usage of the analytical framework, practical cases are considered and a parametric study is conducted to showcase the new perspectives and understanding which would not be possible without the proposed framework.

After a review of actual thermoacoustic devices (e.g. Poese & Garrett 2000; Bassem *et al.* 2011; Backhaus & Swift 2000; Tijani & Spoelstra 2011; Yu *et al.* 2012; Dai *et al.* 2006) available in the literature and the application constraints such as the temperature of low grade heat sources, the typical ranges of the parameters are summarized as follows,

$$R \in [0.05, 0.3]\,\mathrm{mm},\ L \in [10, 50]\,\mathrm{mm},\ T_c \sim 325\,\mathrm{K},\ T_h \in [473, 573]\,\mathrm{K},\ \omega \in [40, 300]\,\pi\mathrm{s}^{-1}$$
$$p_0 \in [0.1, 3]\,\mathrm{MPa},\ |p'|_{\Sigma_1}/p_0 \in [1, 10]\%,\ |p'|_{\Sigma_1}/|(v_z')_{\mathrm{av}}|_{\Sigma_1} \in [1, 30](\rho_0 c)_{\Sigma_1},\ \phi_{vp} \in [-\frac{\pi}{2}, \frac{\pi}{2}].$$

where $T_c = T_w(0)$ and $T_h = T_w(L)$ denote the cold and hot end temperature. The subscript Σ_1 indicates that the flow variable is valued at the inlet surface Σ_1 in figure 2. ϕ_{vp} is a concise notation for the phase difference of $(v_z')_{\mathrm{av}}$ and p' at inlet surface, namely

$$\phi_{vp} := \phi[(v_z')_{\mathrm{av}}]_{\Sigma_1} - \phi[p']_{\Sigma_1}. \tag{4.1}$$

The notation $\phi[f]$ means the phase of a complex quantity f.

The baseline point was chosen to be roughly the mid-points of the ranges for parameters such as R, L, T_h or a moderate value, such as for p_0, that does not demand extreme operating conditions of the device. In this way, it is possible to show the changes towards

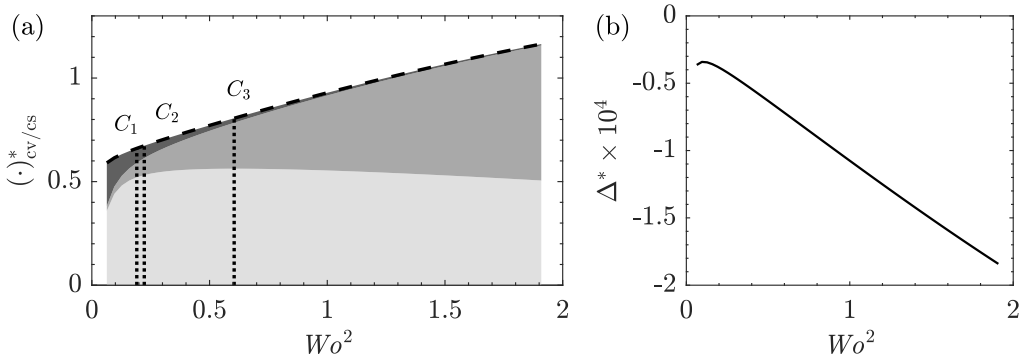

FIGURE 4. The balance of the dimensionless disturbance energy terms against Wo^2. (a) the values of the dimensionless thermoacoustic production in the control volume $(\overline{\mathcal{P}})^*_{\mathrm{cv}}$ (– –), viscous dissipation $(\overline{\mathcal{D}_\nu})^*_{\mathrm{cv}}$ (■), thermal dissipation $(\overline{\mathcal{D}_\nu})^*_{\mathrm{cv}}$ (■) and disturbance energy flux $(\mathbf{n}\cdot\overline{I})^*_{\mathrm{cs}}$ (■) and (b) the deviation from equality defined as $\Delta^* = (\overline{\mathcal{P}})^*_{\mathrm{cv}} - (\overline{\mathcal{D}_\nu})^*_{\mathrm{cv}} - (\overline{\mathcal{D}_\nu})^*_{\mathrm{cv}} - (\mathbf{n}\cdot\overline{I})^*_{\mathrm{cs}}$.

both lower and upper bound of the ranges in the following parametric study. The baseline point was therefore set at $R = 0.15\,\mathrm{mm}$, $L = 30\,\mathrm{mm}$, $T_c = 325\,\mathrm{K}$, $T_h = 523\,\mathrm{K}$, $p_0 = 0.3\,\mathrm{MPa}$, $|p'|_{\Sigma_1}/p_0 = 7\%$, $|(v'_z)_{\mathrm{av}}|_{\Sigma_1} = 3\,\mathrm{ms}^{-1}$, $\phi_{vp} = \frac{\pi}{36}$, $\omega = 200\pi\,\mathrm{s}^{-1}$.

The working fluid was chosen as helium for this parametric study, but the framework is not restricted to this fluid. The dynamic viscosity and thermal conductivity of helium obeys the power laws (Touloukian *et al.* 1975, 1970), $\mu(T) = \mu_{\mathrm{ref}}(T/T_{\mathrm{ref}})^{n_\mu}$ and $k(T) = k_{\mathrm{ref}}(T/T_{\mathrm{ref}})^{n_k}$, respectively, where $T_{\mathrm{ref}} = 300\,\mathrm{K}$, $\mu_{\mathrm{ref}} = 1.9938\times10^{-5}\,\mathrm{kg/ms}$, $k_{\mathrm{ref}} = 0.1524\,\mathrm{W/mK}$, $n_\mu = 0.68014$, $n_k = 0.716$.

The global relative error defined in (3.65) in the baseline case was 5.7×10^{-5} using a equally spaced 201 (radially) × 51 (axially) mesh, showing the suitability of the approach.

4.1. *Parametric Study: Womersley number*

The Womersley number is the most widely discussed dimensionless number in the research of thermoacoustic devices. This is reasonable since it appears both in the dimensionless momentum equation as Wo^2 and energy equation as $Pr\cdot Wo^2$. Although $\mu = \mu(T_0)$ and $k = k(T_0)$, the Prandtl number is very weakly dependent on temperature, varying only by 0.01 in the temperature range [325, 525] K. Therefore the Prandtl number is treated as a constant for helium in this study. Wo^2 being a function of radius, density, frequency and viscosity, can be varied in many ways. In this study, it was varied by changing p_0 and, ultimately, ρ_{ref}, given that $\nabla p_0 = 0$ and $p_0 = \rho_{\mathrm{ref}} R_g T_{\mathrm{ref}}$. Note that $|p'|_{\Sigma_1}$ needed to be changed to keep p'^* constant. It follows that the inlet disturbance energy flux $(\mathbf{n}\cdot\overline{I})_{\Sigma_1}$ used to scale the disturbance energy terms was a linear function of Wo^2.

The terms in the integral disturbance energy balance (3.40) are shown in figure 4 against Wo^2. The vertical heights of light, middle and dark grey area represent respectively dimensionless values of the disturbance energy flux $(\mathbf{n}\cdot\overline{I})^*_{\mathrm{cs}}$, thermal dissipation $(\overline{\mathcal{D}_k})^*_{\mathrm{cv}}$ and viscous dissipation $(\overline{\mathcal{D}_\nu})^*_{\mathrm{cv}}$, of which the sum should equal the thermoacoustic production $(\overline{\mathcal{P}})^*_{\mathrm{cv}}$ (dashed line in figure 4(a)). The deviation from the equality, defined as $\Delta^* = (\overline{\mathcal{P}})^*_{\mathrm{cv}} - (\overline{\mathcal{D}_\nu})^*_{\mathrm{cv}} - (\overline{\mathcal{D}_\nu})^*_{\mathrm{cv}} - (\mathbf{n}\cdot\overline{I})^*_{\mathrm{cs}}$, is plotted in figure 4(b). It can be seen that the difference is 4 orders of magnitude smaller and hence validates the simplification and assumption made previously. In figure 5, $(\overline{\mathcal{D}_\nu})^*_{\mathrm{cv}}$, $(\overline{\mathcal{D}_k})^*_{\mathrm{cv}}$ and total dissipation $(\overline{\mathcal{D}}_{k+\nu})^*_{\mathrm{cv}}$ are shown again for better visualization.

A straightforward yet important conclusion from figure 5(b) is that the relative impor-

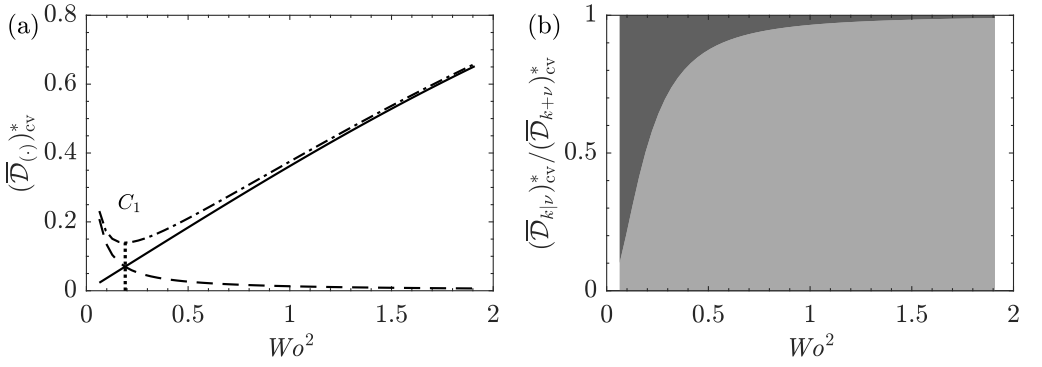

FIGURE 5. The changes of (a) the dimensionless thermal dissipation $(\overline{\mathcal{D}_k})^*_{\mathrm{cv}}$ (—), viscous dissipation $(\overline{\mathcal{D}_\nu})^*_{\mathrm{cv}}$ (– –) and total dissipation $(\overline{\mathcal{D}}_{k+\nu})^*_{\mathrm{cv}}$ (–·–) and (b) the viscous dissipation (■) and thermal dissipation (■) in percentage of the total dissipation against Wo^2.

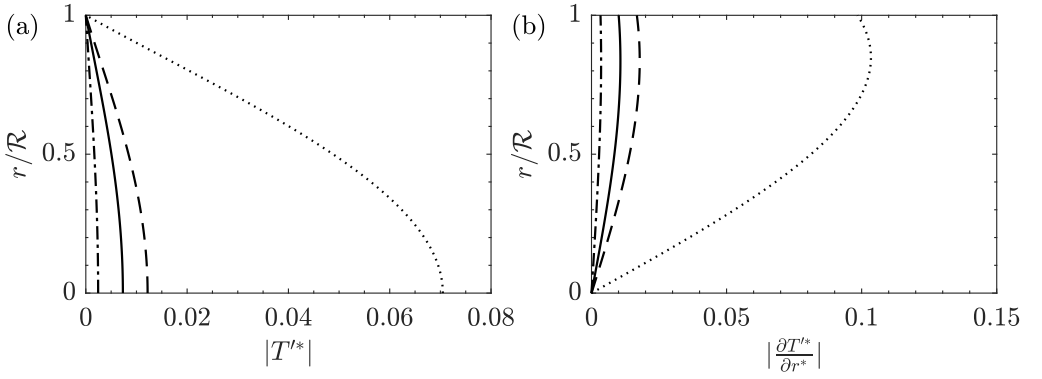

FIGURE 6. The changes of the magnitude of (a) the dimensionless temperature fluctuation $|T'^*|$ and (b) the dimensionless radial derivative of temperature fluctuation $|\frac{\partial T'^*}{\partial r^*}|$ against dimensionless radial position r/R at mid-axial position $z = \frac{L}{2}$ for four different Wo^2: $Wo^2 = 0.06$ (–·–), $Wo^2 = 0.19$ (—), $Wo^2 = 0.32$ (– –), $Wo^2 = 1.9$ (···).

tance of viscous and thermal dissipation, which can be defined as the percentage $\frac{(\overline{\mathcal{D}_\nu})_{\mathrm{cv}}}{(\overline{\mathcal{D}}_{k+\nu})_{\mathrm{cv}}}$ and $\frac{(\overline{\mathcal{D}_k})_{\mathrm{cv}}}{(\overline{\mathcal{D}}_{k+\nu})_{\mathrm{cv}}}$, respectively, shift with Wo^2. When other conditions are maintained, viscous dissipation is more significant at low Wo^2 while thermal dissipation is the main loss mechanism at high Wo^2. This is because Wo, according to equation (3.20), represents the channel radius relative to boundary layer thickness; as the relative radius gets larger, the portion of main flow, which has little velocity gradient, also grows. Hence the relative viscous dissipation drops. For the temperature profile, no oscillation is allowed (i.e. $T' = 0$) at the wall due to the implicit assumption of its infinite heat capacity originated from the boundary condition $T(R, z) = T_w(z)$. As the relative radius gets larger compared to thermal boundary layer, the wall's ability to 'smooth out' the temperature profile decreases as shown in figure 6: the magnitude of temperature oscillation becomes larger and so does its radial gradient. This leads to the surge of thermal dissipation. In summary, figure 5(b) points out the main loss mechanism to tackle when building thermoacoustic devices.

The changes of $(\overline{\mathcal{P}})^*_{\mathrm{cv}}$, $(\overline{\mathcal{D}_\nu})^*_{\mathrm{cv}}$, $(\overline{\mathcal{D}_k})^*_{\mathrm{cv}}$, $(\mathbf{n}\cdot\overline{I})^*_{\mathrm{cs}}$ with Wo^2 can be divided into four regions by three critical values of Wo^2 as labelled in figure 4. With Wo^2 increasing

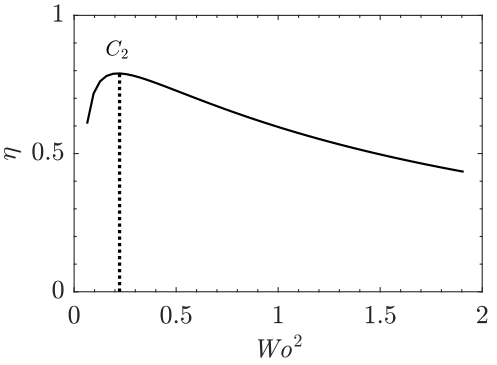

FIGURE 7. The changes of the thermoacoustic efficiency η against Wo^2.

from 0, $(\mathbf{n}\cdot\overline{I})^*_{\mathrm{cs}}$ grows faster than $(\overline{\mathcal{P}})^*_{\mathrm{cv}}$. Given $(\mathbf{n}\cdot\overline{I})^*_{\mathrm{cs}} = (\overline{\mathcal{P}})^*_{\mathrm{cv}} - (\overline{\mathcal{D}}_{k+\nu})^*_{\mathrm{cv}}$, this faster increase of acoustic output clearly benefits from the initial drop of total dissipation as shown in figure 5(a) from 0 to C_1; C_1 is Wo^2 where total dissipation reaches minimum. It follows that C_1 is also the position where $(\overline{\mathcal{P}})^*_{\mathrm{cv}}$ and $(\mathbf{n}\cdot\overline{I})^*_{\mathrm{cs}}$ have parallel tangent lines, i.e. $\mathrm{d}(\overline{\mathcal{P}})^*_{\mathrm{cv}} = \mathrm{d}(\mathbf{n}\cdot\overline{I})^*_{\mathrm{cs}}$. Formally, C_1 is defined as,

$$C_1 = \min\left(Wo^2 : \mathrm{d}(\overline{\mathcal{D}}_{k+\nu})^*_{\mathrm{cv}} = 0\right). \tag{4.2}$$

where the min() function ensures the first such Wo^2. The physical meaning of C_1 is Wo^2 where thermoacoustic production starts to grow faster than acoustic output and where the system has the minimum loss.

Continuing to increase Wo^2, the total dissipation starts to pick up and the rate of change of the production exceeds that of the disturbance energy flux and the second critical value C_2 can be defined as,

$$C_2 = \min\left(Wo^2 : \mathrm{d}\frac{(\mathbf{n}\cdot\overline{I})^*_{\mathrm{cs}}}{(\overline{\mathcal{P}})^*_{\mathrm{cv}}} = 0\right). \tag{4.3}$$

Equivalently, C_2 is also where $\mathrm{dln}(\overline{\mathcal{P}})^*_{\mathrm{cv}} = \mathrm{dln}(\mathbf{n}\cdot\overline{I})^*_{\mathrm{cs}}$. It is clear that this ratio,

$$\eta := \frac{(\mathbf{n}\cdot\overline{I})^*_{\mathrm{cs}}}{(\overline{\mathcal{P}})^*_{\mathrm{cv}}}. \tag{4.4}$$

is the efficiency of the conversion from thermal energy to acoustic energy. Then C_2 is Wo^2 where maximum efficiency is reached. This new definition of 'true' thermoacoustic efficiency reflects only the energy conversion between different aspects of the disturbance and does not concern any steady state physical process. The changes of thermoacoustic efficiency is better visualized in figure 7.

Further increasing Wo^2, it can be seen that both thermoacoustic production and dissipation (mainly thermal) rise sharply. It is clear in figure 4(a) that the $(\mathbf{n}\cdot\overline{I})^*_{\mathrm{cs}}$ has a turning point C_3, i.e. $\mathrm{d}(\mathbf{n}\cdot\overline{I})^*_{\mathrm{cs}} = 0$. It follows that C_3 is also the position where $(\overline{\mathcal{P}})^*_{\mathrm{cv}}$ and $(\overline{\mathcal{D}}_{k+\nu})^*_{\mathrm{cv}}$ have the same rate of change, namely $\mathrm{d}(\overline{\mathcal{P}})^*_{\mathrm{cv}} = \mathrm{d}(\overline{\mathcal{D}}_{k+\nu})^*_{\mathrm{cv}}$. Formally,

$$C_3 = \min\left(Wo^2 : \mathrm{d}(\mathbf{n}\cdot\overline{I})^*_{\mathrm{cs}} = 0\right). \tag{4.5}$$

The physical meaning of C_3 is Wo^2 where $(\mathbf{n}\cdot\overline{I})^*_{\mathrm{cs}}$ reaches the maximum and also where dissipation starts to grow faster than production.

It follows that the four distinct regions are,

- $Wo^2 < C_1$: the total dissipation decreases, the efficiency of the device rises and the energy flux grows faster than the production,

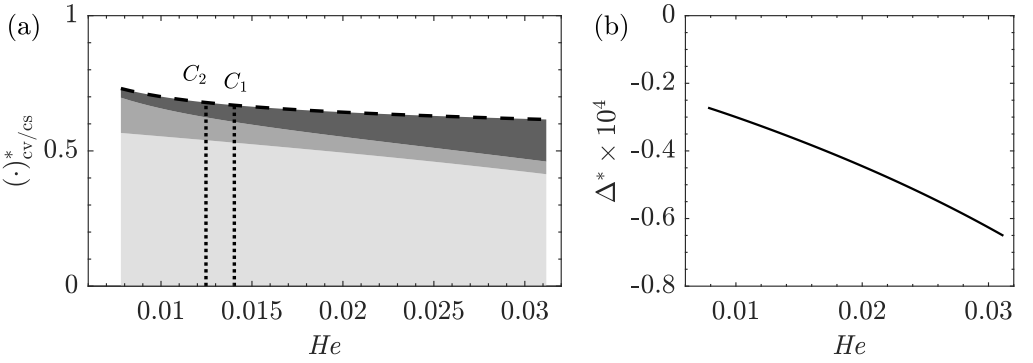

FIGURE 8. The balance of dimensionless disturbance energy terms against He. (a) the values of the dimensionless thermoacoustic production in the control volume $(\overline{\mathcal{P}})^*_{\mathrm{cv}}$ (– –), viscous dissipation $(\overline{\mathcal{D}_\nu})^*_{\mathrm{cv}}$ (■), thermal dissipation $(\overline{\mathcal{D}_\nu})^*_{\mathrm{cv}}$ (■) and disturbance energy flux $(\mathbf{n}\cdot\overline{I})^*_{\mathrm{cs}}$ (■) and (b) the deviation from equality defined as $\Delta^* = (\overline{\mathcal{P}})^*_{\mathrm{cv}} - (\overline{\mathcal{D}_\nu})^*_{\mathrm{cv}} - (\overline{\mathcal{D}_\nu})^*_{\mathrm{cv}} - (\mathbf{n}\cdot\overline{I})^*_{\mathrm{cs}}$.

- $C_1 < Wo^2 < C_2$: efficiency rises, total dissipation rises and production grows faster than energy flux,
- $C_2 < Wo^2 < C_3$: efficiency drops but production grows faster than dissipation, and
- $Wo^2 > C_3$, dissipation rises faster than production.

4.2. *Parametric study: Helmholtz number*

The Helmholtz number represents the length of the channel relative to the wavelength. The thermoacoustic regenerator is generally very short compared with the wavelength: $He \sim O(0.01)$. In this section, the effects of He on disturbance energy budget is studied by varying the channel length L while maintaining other conditions.

The terms in the disturbance energy balance equation are shown in figure 8(a) against the Helmholtz number. Similar to figure 4, the heights of the light, middle and dark grey area represent dimensionless values of disturbance energy flux $(\mathbf{n}\cdot\overline{I})^*_{\mathrm{cs}}$, thermal dissipation $(\overline{\mathcal{D}_k})^*_{\mathrm{cv}}$ and viscous dissipation $(\overline{\mathcal{D}_\nu})^*_{\mathrm{cv}}$, respectively, of which the sum should equal the thermoacoustic production $(\overline{\mathcal{P}})^*_{\mathrm{cv}}$ (dashed line in figure 8). The drop of thermoacoustic production with He is expected because a larger length reduces the temperature gradient. Compared to figure 4, no turning point of $(\mathbf{n}\cdot\overline{I})^*_{\mathrm{cs}}$ is observed in the computed range; $(\mathbf{n}\cdot\overline{I})^*_{\mathrm{cs}}$ decreases monotonically. This result seem to suggest that shorter regenerators are always preferable; however, in practice, the conductivity of the material needs to be taken into account. If the length was too short, most of the heat input would be conducted through the solid wall instead of being transferred to the fluid. The deviation from equality Δ^* against He is shown in figure 8(b); again excellent agreement is seen.

The minimum total dissipation C_1 was obtained at $He = 0.014$, a combined effect of dropping thermal dissipation and rising viscous dissipation with He as shown in figure 9(a). Hence the main loss mechanics for a long regenerator is friction while for short ones it is irreversible heat conduction as visualised in figure 9(b).

The viscous dissipation is expected to rise with increasing He because at high He, the boundary layer extends further in the axial direction, consequently leading to more dissipation. The decline of thermal dissipation with increasing He can be traced back to T'^* as shown in figure 10(a). It is clear magnitude of T'^* diminishes as He increases and, given that R is constant, so does $|\frac{\partial T'^*}{\partial r^*}|$. According to equation (3.43), the thermal dissipation diminishes too.

The thermoacoustic production, by equation (3.46), depends on $|s'^*|$, $|v_z'^*|$, ϕ_{vs}. The

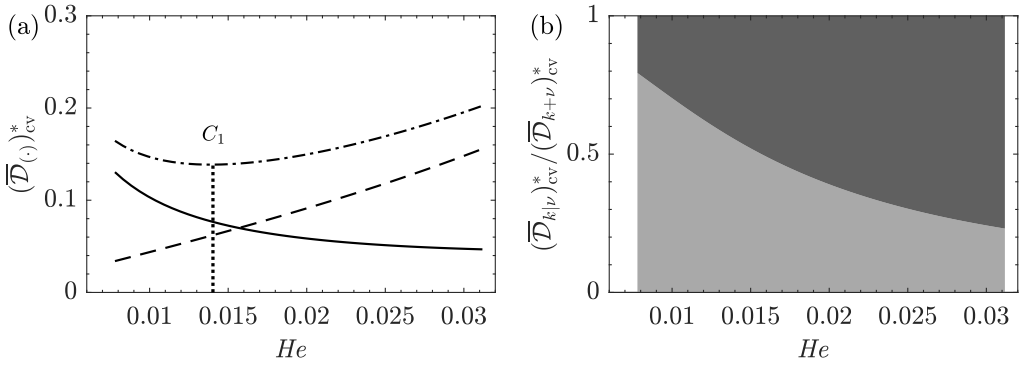

FIGURE 9. The changes of (a) the dimensionless thermal dissipation $(\overline{\mathcal{D}_k})^*_{\mathrm{cv}}$ (—), viscous dissipation $(\overline{\mathcal{D}_\nu})^*_{\mathrm{cv}}$ (– –) and total dissipation $(\overline{\mathcal{D}}_{k+\nu})^*_{\mathrm{cv}}$ (–·–) and (b) the viscous dissipative (■) and thermal dissipation (■) in percentage of total dissipation against He.

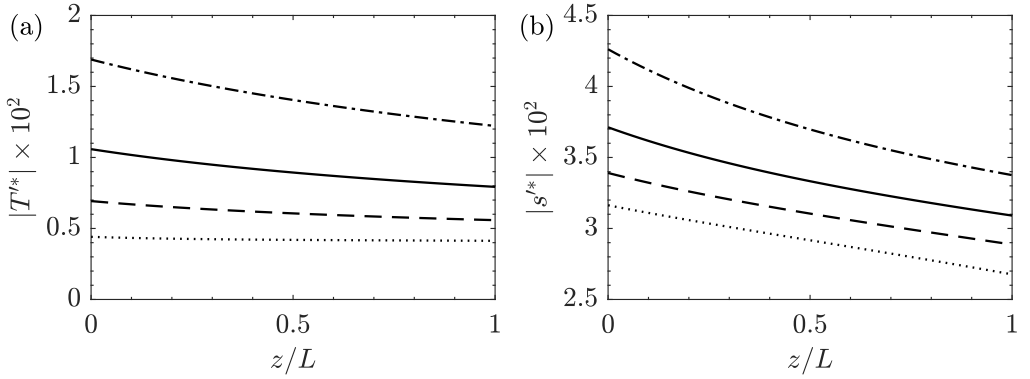

FIGURE 10. The changes of the magnitude of (a) the dimensionless temperature fluctuation $|T'^*|$ and (b) the dimensionless entropy fluctuation $|s'^*|$ against dimensionless axial position z/L on the axis $r = 0$ for four different He: $He = 0.008$ (–·–), $He = 0.012$ (—), $He = 0.019$ (– –), $He = 0.031$ (···).

main contributor in this case was $|s'^*|$, which also drops with increasing He as shown in figure 10(b). This is because, the solutions of T'^* and s'^* are

$$T'^* = \frac{1-\mathcal{H}_k}{\rho_0^*} p'^* - \frac{1}{He^2}\frac{1}{\rho_0^*}\frac{\mathrm{d}T_w^*}{\mathrm{d}z^*}\frac{(1-\mathcal{H}_k)-Pr(1-\mathcal{H}_\nu)}{1-Pr}\frac{\mathrm{d}p'^*}{\mathrm{d}z^*}, \tag{4.6}$$

$$s'^* = \frac{-\mathcal{H}_k}{\rho_0^* T_0^*} p'^* - \frac{1}{He^2}\frac{1}{\rho_0^* T_0^*}\frac{\mathrm{d}T_w^*}{\mathrm{d}z^*}\frac{(1-\mathcal{H}_k)-Pr(1-\mathcal{H}_\nu)}{1-Pr}\frac{\mathrm{d}p'^*}{\mathrm{d}z^*}. \tag{4.7}$$

It can be seen the second parts of the solutions contain $\frac{\mathrm{d}T_w^*}{\mathrm{d}z^*}$; they are the temperature and entropy fluctuation originated from the temperature gradient. In the parametric study, $\frac{\mathrm{d}T_w^*}{\mathrm{d}z^*}$ are identical across He: same cold and hot temperature varying linearly form 0 to 1. It is He that accounts for the temperature gradient changes in the dimensionless domain. Since both solutions contain the inverse of He, the magnitudes drop with increasing He.

The thermoacoustic efficiency η is shown against He in figure 11. Although there exists the highest efficiency C_2 at $He = 0.012$, the change of the efficiency is rather insensitive to He compared with that against Wo^2 in figure 7. This indicates that as long as He is small ($\sim O(0.01)$), the effect of the channel length (and consequently temperature

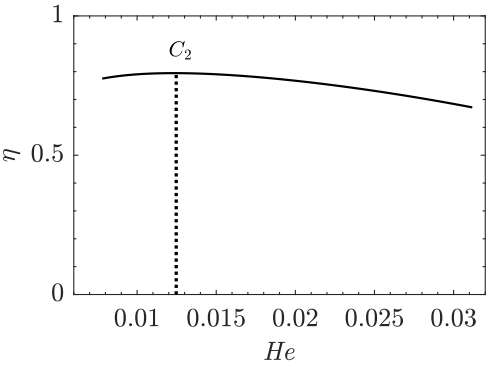

FIGURE 11. The changes of the thermoacoustic efficiency against He.

gradient) on the efficiency is less important than the effects of shear and heat transfer in the radial direction.

As mentioned previously, the wave growth decreases monotonically with larger He; in practice the choice of ω and L should ideally be such that the resulting He falls to the left of C_1, i.e. $He < C_1$, taking advantage of both high efficiency and high output.

4.3. *Two dimensional variation*

Up to this point, the global values (volume integral $(\overline{\mathcal{P}})^*_{\mathrm{cv}}$, $(\overline{\mathcal{D}_k})^*_{\mathrm{cv}}$, $(\overline{\mathcal{D}_\nu})^*_{\mathrm{cv}}$ and surface integral $(\mathbf{n}\cdot\overline{I})^*_{\mathrm{cs}}$) and the integral form of the disturbance energy balance relation (3.34) have been used. In this section, the differential form of disturbance energy (2.27) is employed to analyse the two dimensional variation of the point-based values $(\overline{\mathcal{P}})^*$, $(\nabla\cdot\overline{I})^*$, $(\overline{\mathcal{D}_k})^*$ and $(\overline{\mathcal{D}_\nu})^*$.

Compared with previous 1D models, one of the highlights of this work is that the problem is considered in an axisymmetric cylindrical domain. Hence, this work is capable of showing the two dimensional variation of the disturbance energy terms against radial and axial location. The profiles of $(\overline{\mathcal{P}})^*$, $(\nabla\cdot\overline{I})^*$, $(\overline{\mathcal{D}_k})^*$, and $(\overline{\mathcal{D}_\nu})^*$ are given in figure 12. The vertical axis is the dimensionless radius $r^* = r/R$ where $r^* = 0$ represents the axis and $r^* = 1$ is the wall.

Focus first on the radial variation. At the wall, $(\overline{\mathcal{P}})^*$ is zero because $v_z'^*$ is zero (non-slip boundary condition). The $(\overline{\mathcal{D}_\nu})^*$ and $(\overline{\mathcal{D}_k})^*$ are significant because $|\frac{\partial T'^*}{\partial r^*}|$ and $|\frac{\partial v_z'^*}{\partial r^*}|$ are both large at the wall. Consequently, the near-wall region actually sees a negative energy flux density $(\nabla\cdot\overline{I})^* = (\overline{\mathcal{P}})^* - (\overline{\mathcal{D}}_{k+\nu})^* < 0$, representing a wave decay. The $(\nabla\cdot\overline{I})^* = 0$ level mark is shown in figure 12(c) for clearer visualization. It is interesting to realize that even for thermoacoustic devices designed to amplify the waves, a small region of wave decay always exists. The near-wall wave decay also provides support to the conclusion in section 4.1 that overly small Wo^2 is not optimal. On the axis, $(\overline{\mathcal{P}})^*$ reaches the maximum while dissipation is zero (axisymmetric condition) and hence $(\nabla\cdot\overline{I})^* = (\overline{\mathcal{P}})^*$ on the axis. The fact that wave growth is uneven in the radial direction implies the presence of the radial mixing loss associated with fluid near both ends entering and leaving the channels during oscillation.

With regards to the axial variation, it is too simplistic to assume the shapes of the profiles are self-similar. Take $\overline{\mathcal{P}}$ for example. Normalise each profile using respective values on the axis as shown in figure 13. It can be seen that the profiles are almost self-similar but not quite. This is because radial distribution functions contain the local viscous and thermal boundary layer thickness δ_ν and δ_k, which ultimately depend on $T(z)$.

The axial changes were monotonic: $(\overline{\mathcal{P}})^*$, $(\overline{\mathcal{D}_k})^*$, $(\nabla\cdot\overline{I})^*$ dropped as the axial location

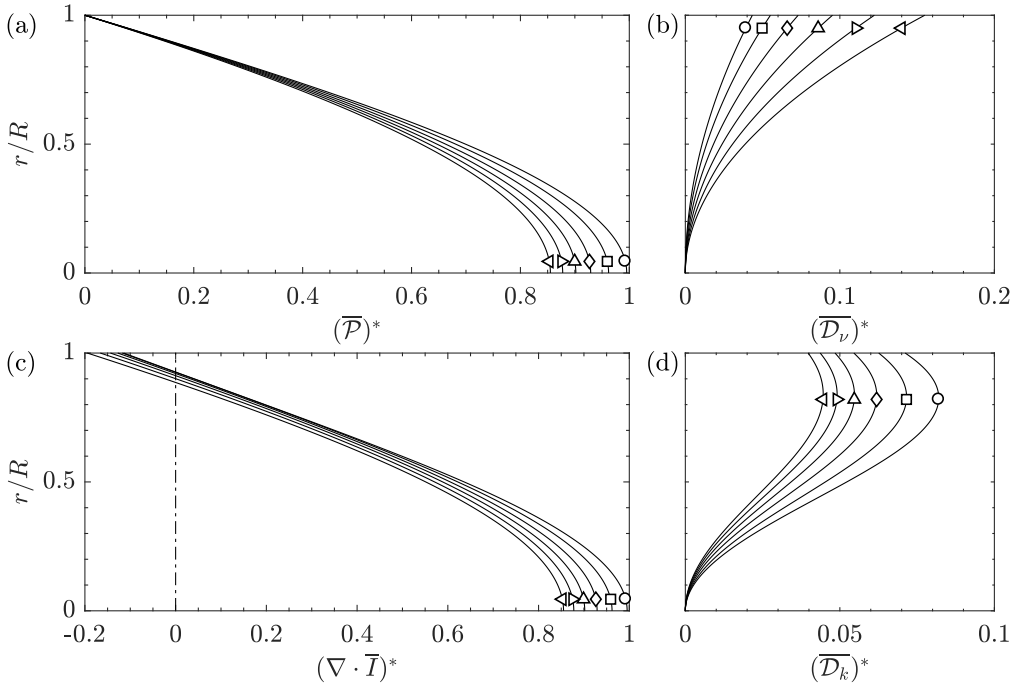

FIGURE 12. The profiles of the cycle-averaged (a) dimensionless thermoacoustic production $(\overline{\mathcal{P}})^*$, (b) viscous dissipation $(\overline{\mathcal{D}_\nu})^*$, (c) disturbance energy flux density $(\nabla \cdot \overline{I})^*$ and (d) thermal dissipation $(\overline{\mathcal{D}_k})^*$ at six axial locations: $z/L = 0.02, 0.2, 0.4, 0.6, 0.8, 0.98$ which are denoted by ○, □, ◊, △, ▷, ◁, respectively, at the baseline point.

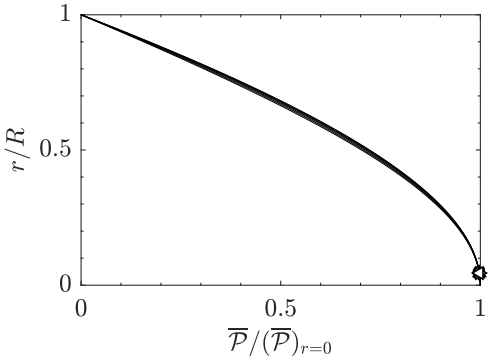

FIGURE 13. The profiles of the thermoacoustic production normalised by its value on the axis $\overline{\mathcal{P}}/(\overline{\mathcal{P}})_{r=0}$ against dimensionless radial position r/R at six axial locations: $z/L = 0.02, 0.2, 0.4, 0.6, 0.8, 0.98$ which are denoted by ○, □, ◊, △, ▷, ◁, respectively, at the baseline point.

moves towards the hot end; on the contrary, $(\overline{\mathcal{D}_\nu})^*$ increased. Recalling equation (3.45) and (3.43), the changes of $(\overline{\mathcal{D}_k})^*$ and $(\overline{\mathcal{D}_\nu})^*$ are readily explained by the profiles of $|\frac{\partial T'^*}{\partial r^*}|$ and $|\frac{\partial v_z'^*}{\partial r^*}|$ as shown in figure 14. Note that although $k(T_w(z))$ increased with axial location (actually $k(L) = 1.41k(0)$), the factor $k^*\frac{1}{T_0^*}$ in (3.43) actually dropped with axial location given the power law $k \propto T^{0.716}$ as mentioned previously.

By referring to the thermoacoustic production (3.46), the effect of $\frac{\mathrm{d}T_0^*}{\mathrm{d}z^*}$ vanished here by

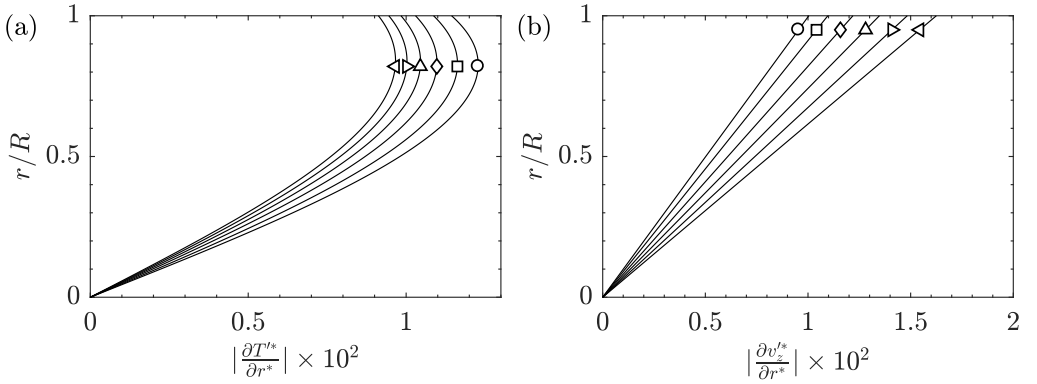

FIGURE 14. The profiles of the magnitude of (a) the dimensionless radial derivative of temperature fluctuation $|\frac{\partial T'^*}{\partial r^*}|$ and (b) the dimensionless radial derivative of axial velocity fluctuation $|\frac{\partial v_z'^*}{\partial r^*}|$ against dimensionless radial position r/R at six axial locations: $z/L = 0.02, 0.2, 0.4, 0.6, 0.8, 0.98$ which are denoted by ○, □, ◊, △, ▷, ◁, respectively, at the baseline point.

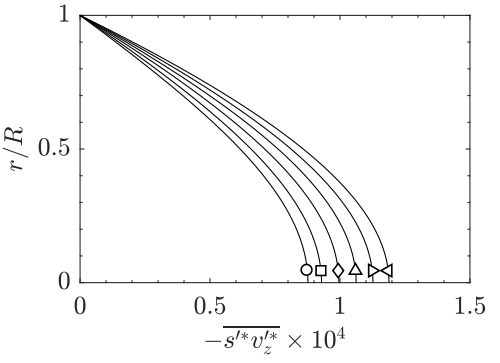

FIGURE 15. The profiles of the cycle-averaged product of dimensionless fluctuating entropy and axial velocity $-\overline{s'^* v_z'^*}$ against dimensionless radial position r/R at six axial locations: $z/L = 0.02, 0.2, 0.4, 0.6, 0.8, 0.98$ which are denoted by ○, □, ◊, △, ▷, ◁, respectively, at the baseline point.

the choice of linear temperature distribution. The factor $-\overline{s'^* v_z'^*}$ is the specific entropy transported by the volumetric flow rate per unit area per unit time. The profiles of $-\overline{s'^* v_z'^*}$ are shown in figure 15. It is clear that $-\overline{s'^* v_z'^*}$ increased as axial position moves towards the hot end. However, this trend was reversed by ρ_0^*, which decreases with z.

In summary, it has been shown that there is a near-wall wave decay region and the two dimensional variation of $(\overline{\mathcal{P}})^*$, $(\nabla \cdot \overline{I})^*$, $(\overline{\mathcal{D}_k})^*$ and $(\overline{\mathcal{D}_\nu})^*$ can be summarized as similar radial profiles and monotonic axial changes.

5. Conclusions

In this work, a new analytical framework has been developed to better understand the disturbance energy balance in thermoacoustic devices. In this framework, a thermoacoustic production term is newly proposed which directly quantifies the generation or consumption of disturbance energy from an imposed temperature gradient. An extended disturbance energy flux term, in place of acoustic intensity, is defined to account for wave

growth or decay in thermoacoustic devices. The viscous and thermal dissipation solely resulting from the gradients of fluctuating velocity and temperature are obtained. The disturbance energy balance relation is then established, stating that the wave growth equals thermoacoustic production less viscous and thermal dissipation. The proposed framework enables a new analytical perspective using these four disturbance energy terms and the changes of the balance itself. Both the differential and integral form of disturbance energy balance equation are given.

In this study, the framework has been implemented in an axisymmetric cylindrical domain. The governing equations have been non-dimensionalised and the driving dimensionless parameters, namely the Womersley number, the Helmholtz number and the Prandtl number are revealed. The well-accepted Rott's assumptions were re-interpreted using order of magnitude analysis. The disturbance energy terms are then simplified by extending the Rott's assumptions and taking advantage of boundary conditions. The flow variables have been solved analytically in the radial direction and numerically in the axial direction. A global error of the disturbance energy balance has been defined to validate the assumptions made and the numerical scheme used in this study. Compared with previous 1D models, one of the highlights of this work is the ability to show two dimensional variations. It has been found the disturbance energy terms have similar but not strictly self-similar radial shapes and monotonic axial changes. It has been discovered that the wave always decays in the region close to wall, which implies extra mixing loss that 1D models fail to see.

In order to showcase the new perspectives enabled by the proposed framework, a parametric study of the Womersley and Helmholtz number has been conducted. The study is not intended to be exhaustive but to demonstrate how new physical insights and design guideline can be obtained from the disturbance energy balance relation. The findings are:

(i) The Womersley and Helmholtz number can be interpreted as the channel radius relative to boundary layer thickness and the channel length relative to the wavelength, respectively. It has been found that for a relatively wide channel (represented by a large Womersley number) or short channel (small Helmholtz number), the major loss mechanism is thermal dissipation; in both case this is due to substantial temperature fluctuation. For a relatively narrow or long regenerator channel, viscous dissipation dominates. The significance of thermal dissipation in thermoacoustic devices has become clear for the first time.

(ii) This paper answers the question of what the 'true' thermoacoustic efficiency is. A new thermoacoustic efficiency has been defined as the ratio of wave growth to thermoacoustic disturbance production; it reflects only the energy conversion between different aspects of the disturbance and does not concern any steady state physical process.

(iii) The change of thermoacoustic efficiency is rather insensitive to the Helmholtz number compared to the Womersley number. This indicates that as long as the regenerator is short compared to the waves ($He \sim O(0.01)$), the effect of the channel length (and consequently temperature gradient) on the efficiency is less important than the effects of momentum and thermal diffusion in the radial direction.

(iv) Three critical design values are identified: the minimum of dimensionless total dissipation, the maximum of thermoacoustic efficiency and the maximum of dimensionless wave growth. These three critical values divided the parameter space into four regimes; a designer can wisely pick the combination of geometry, wave properties and working conditions according to the preference of efficiency, output and loss.

REFERENCES

Akhavan, R., Kamm, R. D. & Shapiro, A. H. 1991 An investigation of transition to turbulence in bounded oscillatory stokes flows .1. experiments. *Journal of Fluid Mechanics* **225**, 395–422.

Backhaus, S. & Swift, G. W. 1999 A thermoacoustic stirling heat engine. *Nature* **399** (6734), 335–338.

Backhaus, S. & Swift, G. W. 2000 A thermoacoustic-stirling heat engine: Detailed study. *Journal of the Acoustical Society of America* **107** (6), 3148–3166.

Bassem, M. M., Ueda, Y. & Akisawa, A. 2011 Design and construction of a traveling wave thermoacoustic refrigerator. *International Journal of Refrigeration-Revue Internationale Du Froid* **34** (4), 1125–1131.

Cao, N., Olson, J. R., Swift, G. W. & Chen, S. 1996 Energy flux density in a thermoacoustic couple. *Journal of the Acoustical Society of America* **99** (6), 3456–3464.

Chu, B.-T. 1965 On the energy transfer to small disturbances in fluid flow (part i). *Acta Mechanica* **1** (3), 215–234.

Dai, W., Luo, E. C., Zhang, Y. & Ling, H. 2006 Detailed study of a traveling wave thermoacoustic refrigerator driven by a traveling wave thermoacoustic engine. *The Journal of the Acoustical Society of America* **119** (5), 2686–2692.

Dowling, A. P. & Stow, S. R. 2003 Acoustic analysis of gas turbine combustors. *Journal of Propulsion and Power* **19** (5), 751–764.

Giauque, A., Poinsot, T., Brear, M. & Nicoud, F. 2006 Budget of disturbance energy in gaseous reacting flows. In *Proc. of the Summer Program*, pp. 285–297. Center for Turbulence Research, NASA Ames/Stanford Univ.

Hairer, E., Nørsett, S. P. & Wanner, G. 1993 *Solving Ordinary Differential Equations I (2nd Revised. Ed.): Nonstiff Problems*. Berlin, Heidelberg: Springer-Verlag.

Hino, M., Sawamoto, M. & Takasu, S. 1976 Experiments on transition to turbulence in an oscillatory pipe-flow. *Journal of Fluid Mechanics* **75** (May27), 193–207.

In't Panhuis, P. H. M. W., Rienstra, S. W., Molenaar, J. & Slot, J. J. M. 2009 Weakly nonlinear thermoacoustics for stacks with slowly varying pore cross-sections. *Journal of Fluid Mechanics* **618**, 41–70.

Karimi, N., Brear, M. J. & Moase, W. H. 2008 Acoustic and disturbance energy analysis of a flow with heat communication. *Journal of Fluid Mechanics* **597**, 67–89.

Karpov, S. & Prosperetti, A. 2002 A nonlinear model of thermoacoustic devices. *The Journal of the Acoustical Society of America* **112** (4), 1431–1444.

Lieuwen, T. C. & Yang, V. 2005 *Combustion instabilities in gas turbine engines: operational experience, fundamental mechanisms, and modeling*. American Institute of Aeronautics and Astronautics.

Merkli, P. & Thomann, H. 1975 Thermoacoustic effects in a resonance tube. *Journal of Fluid Mechanics* **70** (01), 161–177.

Myers, M. K. 1991 Transport of energy by disturbances in arbitrary steady flows. *Journal of Fluid Mechanics* **226**, 383–400.

Nicoud, F. & Poinsot, T. 2005 Thermoacoustic instabilities: Should the rayleigh criterion be extended to include entropy changes? *Combustion and Flame* **142** (1-2), 153–159.

Ohmi, M., Iguchi, M., Kakehashi, K. & Masuda, T. 1982 Transition to turbulence and velocity distribution in an oscillating pipe-flow. *Bulletin of the Jsme-Japan Society of Mechanical Engineers* **25** (201), 365–371.

Pierce, A. D. 1981 *Acoustics: an introduction to its physical principles and application*. New York ; London: McGraw-Hill.

Poese, M. E. & Garrett, S. L. 2000 Performance measurements on a thermoacoustic refrigerator driven at high amplitudes. *The Journal of the Acoustical Society of America* **107** (5), 2480–2486.

Prince, P. J. & Dormand, J. R. 1981 High order embedded runge-kutta formulae. *Journal of Computational and Applied Mathematics* **7** (1), 67 – 75.

Rott, N. 1969 Damped and thermally driven acoustic oscillations in wide and narrow tubes. *Zeitschrift für angewandte Mathematik und Physik ZAMP* **20** (2), 230–243.

Rott, N. 1975 Thermally driven acoustic oscillations, part iii: second-order heat flux. *Zeitschrift für angewandte Mathematik und Physik ZAMP* **26** (1), 43–49.

Scalo, C., Lele, S. K. & Hesselink, L. 2015 Linear and nonlinear modelling of a theoretical travelling-wave thermoacoustic heat engine. *Journal of Fluid Mechanics* **766**, 368–404.

Swift, G. W. 1988 Thermoacoustic engines. *The Journal of the Acoustical Society of America* **84** (4), 1145–1180.

Swift, G. W. 2002 *Thermoacoustics: A unifying perspective for some engines and refrigerators*. Acoustical Society of America.

Tijani, M. E. H. & Spoelstra, S. 2011 A high performance thermoacoustic engine. *Journal of Applied Physics* **110** (9).

Tominaga, A. 1995 Thermodynamic aspects of thermoacoustic theory. *Cryogenics* **35** (7), 427–440.

Touloukian, Y, S., Liley, P. E. & Saxena, S. C. 1970 Thermophysical properties of matter-the tprc data series. volume 3. thermal conductivity-nonmetallic liquids and gases. *Tech. Rep.*. Purdue University.

Touloukian, Y. S., Saxena, S. C. & Hestermans, P. 1975 Thermophysical properties of matter-the tprc data series. volume 11. viscosity. *Tech. Rep.*. Purdue University.

Worlikar, Aniruddha S. & Knio, Omar M. 1996 Numerical simulation of a thermoacoustic refrigerator. *Journal of Computational Physics* **127** (2), 424 – 451.

Wu, Z. H., Zhang, L. M., Dai, W. & Luo, E. C. 2014 Investigation on a 1 kw traveling-wave thermoacoustic electrical generator. *Applied Energy* **124**, 140–147.

Yu, Z. B., Jaworski, A. J. & Backhaus, S. 2012 Travelling-wave thermoacoustic electricity generator using an ultra-compliant alternator for utilization of low-grade thermal energy. *Applied Energy* **99**, 135–145.

Declaration of Interests

The authors report no conflict of interest.